Tectonophysics 680 (2016) 67–89

Contents lists available at ScienceDirect

Tectonophysics

journal homepage: www.elsevier.com/locate/tecto

Seismic sources and stress transfer interaction among axial normal faults and external thrust fronts in the Northern Apennines (Italy): A working hypothesis based on the 1916–1920 time–space cluster of earthquakes

Marco Bonini [a,*], Giacomo Corti [a], Dario Delle Donne [b], Federico Sani [c], Luigi Piccardi [a], Gianfranco Vannucci [d], Riccardo Genco [c], Luca Martelli [e], Maurizio Ripepe [c]

[a] CNR, Consiglio Nazionale delle Ricerche, Istituto di Geoscienze e Georisorse, UOS Firenze, Via G. La Pira, 4, 50121 Firenze, Italy
[b] Dipartimento di Scienze della Terra e del Mare (DiSTeM), Università degli Studi di Palermo, Via Archirafi, 36, 90123 Palermo, Italy
[c] Dipartimento di Scienze della Terra, Università degli Studi di Firenze, Via G. La Pira, 4, 50121 Firenze, Italy
[d] INGV, Istituto Nazionale di Geofisica e Vulcanologia, Via D. Creti, 12, 40128 Bologna, Italy
[e] Regione Emilia-Romagna, Servizio Geologico, Sismico e dei Suoli, Viale A. Silvani 4/3, 40122 Bologna, Italy

ARTICLE INFO

Article history:
Received 30 June 2015
Received in revised form 27 April 2016
Accepted 30 April 2016
Available online 6 May 2016

Keywords:
Northern Apennine
1916–1920 earthquake cluster
Seismic sources
Axial normal faults
External thrust fronts
Static stress transfer

ABSTRACT

In this study we analyse the main potential seismic sources in some axial and frontal sectors of the Northern Apennines, in Italy. This region was hit by a peculiar series of earthquakes that started in 1916 on the external thrust fronts near Rimini. Later, in 1917–1921, seismicity (up to Mw ≈ 6.5) shifted into the axial zone and clearly migrated north-westward, along the belt of active normal faults. The collection of fault-slip data focused on the active normal faults potentially involved in this earthquake series. The acquired data allowed us to better characterize the geometry and kinematics of the faults. In a few instances, the installation of local seismic networks during recent seismic sequences allowed the identification of the causative faults that are hinted to be also responsible for past earthquakes, particularly in the Romagna region and north-eastern Mugello. The Coulomb stress changes produced by the historical earthquakes generally brought closer to failure all the faults that supposedly caused the main seismic events of 1916–1921. However, the stress change magnitude is generally small and thus the static stress interaction among the main seismic sources is not supported by a significant seismic correlation. Significant stress change loading may be instead inferred for the triggering of a number of seismic events on neighbouring normal faults by the Garfagnana 1920 earthquake. In addition, the computation of the seismic stress changes suggests that seismic events with magnitude ≥ 6 may transmit stresses from the axial normal faults to specific external thrusts and vice versa. It is possible that a correlation may be made between loading applied by the major 1917–1920 extensional ruptures and the increased seismicity on the distal external thrusts.

1. Introduction

Long-term seismic activity is clearly governed by geodynamic processes resulting from interactions along plate boundaries. On the other hand, different seismic sources may interact with each other in the short-to-middle term by transferring static and dynamic stresses produced during earthquakes. Mutual interaction and stress transfer between seismogenic structures with different kinematics and also between faults and volcanoes have long been identified (e.g., King et al., 1994; Nostro et al., 1998; Lin and Stein, 2004; Lin et al., 2011). Here, we focus on the Northern Apennines fold-and-thrust belt, where the seismicity is essentially caused by active thrusting along the external Adriatic fronts and by normal faulting along the axial zone of the belt, which is about 40–60 km far from the former sector (Fig. 1a; e.g., Basili et al., 2008; DISS Working Group, 2015). The axial sector is characterized by a belt of Quaternary intramontane basins that bound the main watershed to the southwest. This area represents the major seismic zone of the Northern Apennines, where a few historical earthquakes have reached a macroseismically-derived magnitude of Mw ≈ 6.5 (Rovida et al., 2011). The highest macroseismic magnitude estimated along the external thrust fronts is of Mw ≈ 6.1 instead.

A sequence of moderate-to-strong seismic events hit the Northern Apennines and clustered in the period between 1916 and 1920 (Fig. 1b). This earthquake cluster started with an intense series of earthquakes along the external compressive fronts, which culminated in two main seismic events of Mw ≈ 6–6.1 (May and August 1916). The location of the main shocks then shifted into the axial sector: here the main seismic events showed a clear time–space migration from southeast to northwest, as indicated by the macroseismically-derived earthquake

* Corresponding author.
E-mail addresses: mbonini@igg.cnr.it, mbonini@geo.unifi.it (M. Bonini).

http://dx.doi.org/10.1016/j.tecto.2016.04.045
0040-1951/

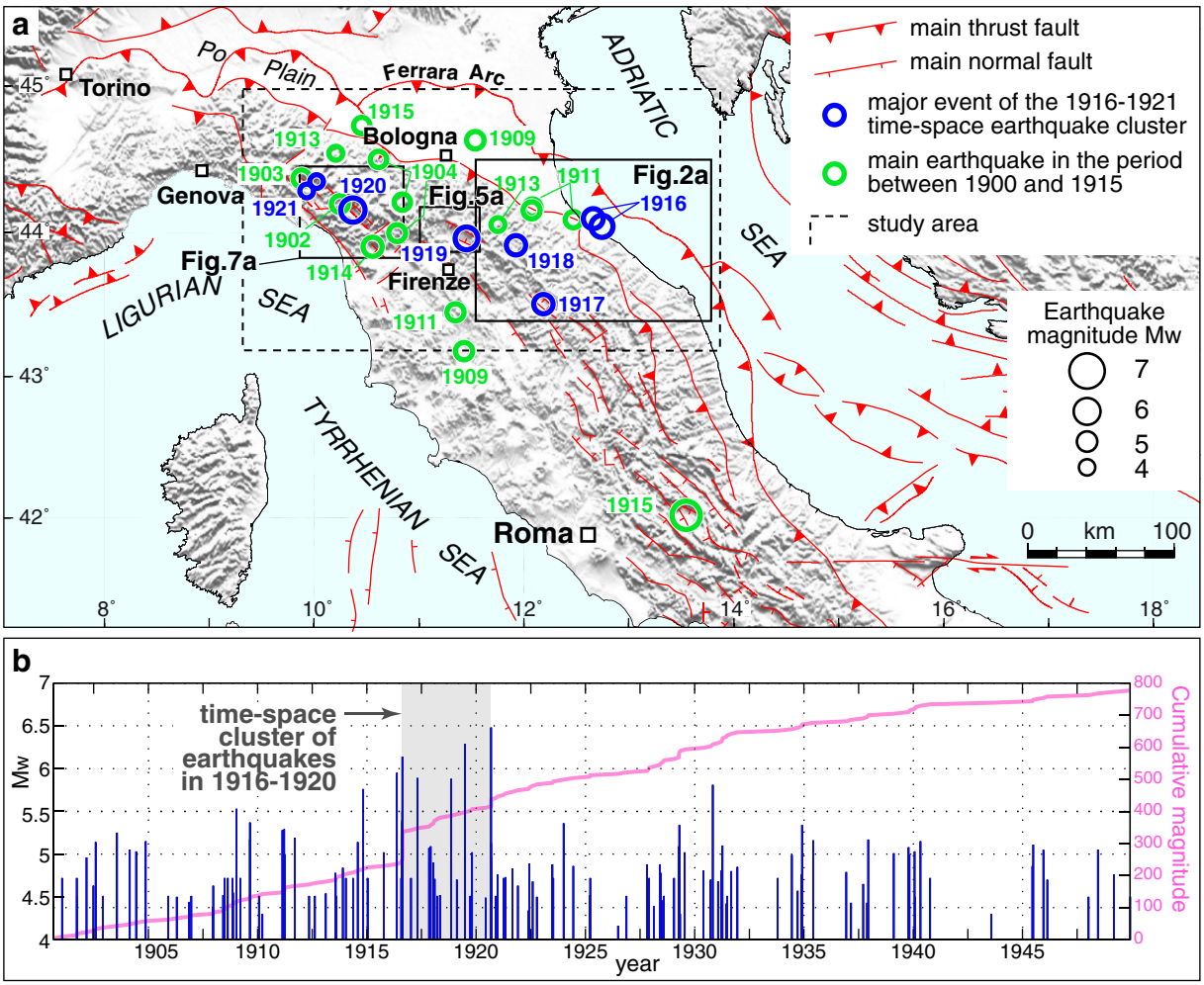

Fig. 1. Time–space cluster of earthquakes that hit the Northern Apennines (Italy) between 1916 and 1921. The open blue circles indicate the epicentres of the 1916–1921 main earthquakes. The open green circles indicate the main seismic events (Mw ≥ 5 ± 0.25) within the study area (dashed black box) in the period between 1900 and 1915 (thus before the main 1916–1921 earthquake cluster) (macroseismic data from Rovida et al., 2011). (b) Magnitude Mw of earthquakes in the period between 1900 and 1950 in the Northern Apennines, plotted against the cumulative magnitude (purple line). Note the marked step in the cumulative magnitude in 1916. The seismicity is calculated over the study area (dashed black box in panel a).

parameters (CPTI11; Rovida et al., 2011) by using the boxer code after Gasperini et al. (1999, 2010). These events are represented by the Mw ≈ 5.9 Valtiberina earthquake of April 26, 1917, the Mw ≈ 5.9 Romagna earthquake of November 10, 1918, the Mw ≈ 6.3 Mugello earthquake of June 29, 1919, and the Mw ≈ 6.5 Garfagnana earthquake of September 7, 1920 (Fig. 1a). Two earthquakes with Mw ≈ 4.7 occurred in 1921 northwest of Garfagnana (Lunigiana). Although their magnitude is smaller than that of the 1917–1920 events, they denote a clear progression of the normal faulting toward the northwest (Fig. 1a). Therefore we consider such events as the continuation of the series of earthquakes along the axial zone.

The large release of seismic energy in such a relatively short time span may suggest an interaction among the various seismic sources, and also indicate that the main earthquakes of the cluster were triggered in some ways by previous events. In particular, published numerical models (Viti et al., 2012) of elastic-viscous post-seismic relaxation have taken into account the role of the Mw ≈ 7.0 Avezzano earthquake that struck the Fucino basin (in the central Apennines) on January 13 1915. This seismic event occurred more than 200 km south of the fault that ruptured in 1917 (Fig. 1a), and the results of numerical modelling allowed the assumption that the Avezzano earthquake caused a significant increase of seismicity in the Northern Apennines (Viti et al., 2012), possibly in relation to a long-distance interaction between seismic sources (Mantovani et al., 2010). There is also a growing body of evidence suggesting that small permanent static stress changes in the crust due to an earthquake can accelerate the failure of neighbouring faults and trigger aftershocks and large earthquake sequences up to few fault lengths away from the epicentre area (e.g., King et al., 1994; Stein, 1999). In the present work, we explore the role that static stress changes may have played in the activation of the earthquake cluster in 1916–1921 and successive seismic events. Our aim is to use the knowledge gained from analysing the past events to develop improved future scenarios. This study may be relevant in helping understanding how earthquakes may influence the development of other earthquakes. More specifically, this study aims to explore the mutual relationships between the generation of normal earthquakes in the axial zone and the earthquakes on the external thrusts.

After reviewing the main seismic sources involved in the considered series of seismic events, we describe the method, and then we proceed in assessing the possible interactions between axial normal faults and external thrusts, and the relative roles of static stress changes.

2. Methods

2.1. Coulomb models, assumptions and limitations

The change in Coulomb failure stress caused by earthquakes on other faults is expressed in the Coulomb Failure Function (e.g., Stein et al., 1992; Reasenberg and Simpson, 1992; King et al., 1994; Harris, 1998; Stein, 1999; Cocco and Rice, 2002; Kilb et al., 2002) as:

$$\Delta CFF = \Delta\tau + \mu(\Delta\sigma_n + \Delta P), \quad (1)$$

where $\Delta\tau$ and $\Delta\sigma_n$ are respectively the shear and normal stress change components acting on the 'receiver' fault, μ is the friction coefficient and ΔP is the change in pore pressure within the fault. The change in Coulomb failure stress is commonly rewritten as (King, 2014, and references therein):

$$\Delta CFF = \Delta\tau + \mu'\Delta\sigma_n \quad (2)$$

where μ' is the apparent coefficient of friction that comprises the role of pore fluid pressure as well as the material properties of the fault zone. The Coulomb stress change is therefore the algebraic sum of the changes in shear stress and normal stress that promote (ΔCFF positive) or inhibit (ΔCFF negative) shear failure on a given fault set. The distribution pattern of increases and decreases of Coulomb stress changes commonly shows fault-end and off-fault stress lobes (e.g., King, 2014). Stresses are computed in a homogeneous elastic half-space (Okada, 1992), in which the elastic body is assumed to have the following properties (based on King et al., 1994; Lin and Stein, 2004; Toda et al., 2005, 2011): Poisson's ratio $\nu = 0.25$, Young's modulus $E = 8 \times 10^5$ bar (implying shear modulus, $G = 3.2 \times 10^5$ bar). The apparent coefficient of friction is assumed as 0.4, which is the average in the 0.0–0.8 range of possible values (King et al., 1994). The shear and normal stresses produced by a 'source' earthquake are resolved onto specific 'receiver' faults, which are defined by their strike, dip, and rake. The source faults are assumed with tapered slip to prevent unrealistically high stress concentration at the edges of the fault. The calculations of Coulomb stress changes were performed using the Coulomb 3.4 software (http://www.coulombstress.org; Toda et al., 2011). The analyses of seismic sequences indicate that aftershocks can be promoted or halted by stress changes of just ± 0.1 bar (10 kPa), with delays in the response that may vary from seconds to years (e.g., Reasenberg and Simpson, 1992; King et al., 1994; Stein, 1999). In some cases even the small stresses produced by solid Earth tides (~0.01 bar) appear to play a role in the triggering of earthquakes (e.g., Cochran et al., 2004; Tanaka et al., 2004; Métivier et al., 2009).

A number of assumptions and simplifications were introduced in the computation, specifically the one considering the system as a homogeneous and linearly elastic material. In addition, the results may be affected by uncertainties related to hypocentre and epicentre location, the precise earthquake magnitude, and the geometry and kinematics of the causative fault (i.e., rake, dip or strike). Therefore, even small differences in the parameters of the fault source may have a significant impact on the calculation of the static stress changes. This problem is particularly evident for historical earthquakes whose instrumental data are lacking and whose location is generally known with the limited accuracy typical of macroseismic data. In particular, in the near field the uncertainty in the macroseismic localization may lead to extremely different and contrasting results, whereas these effects are more limited in the far field. For this reason, we have not calculated static stress changes for historical seismic events whose epicenters fall along the boundary between positive and negative lobes of the Coulomb stress changes.

Another shortcoming in this analysis is the hypocentral depth, which is generally not included in the CPTI11 catalogue (Rovida et al., 2011) that has provided the macroseismic magnitude of the historical earthquakes considered in this study. The hypocentral depth represents, therefore, an important source of uncertainty when evaluating historical earthquakes. We have tackled this problem by conducting a sensitivity analysis that consisted in the iterative calculation of the Coulomb stress changes at the upper and lower boundaries of a potential seismogenic layer, referred to respectively as D^1 and D^2. The upper (shallower) boundary D^1 has been fixed at 4.5 km depth, based on the hypocentres calculated for some of the historical earthquakes considered in this study (i.e., the 1920 Garfagnana event; Solarino, 2005). The lower (deeper) boundary D^2 is calculated from the 75% of seismicity cutoff at depth, taking into consideration the seismic events falling in cells with 0.1° of latitude and longitude. Importantly, the 75% cutoff has been documented to be reliable for establishing the vertical extent of the seismogenic layer in the Northern Apennines (Chiarabba et al., 2005). For the more external thrust faults the depth of the seismogenic layer computed by the cut-off of seismicity appears to be less constrained (Chiarabba et al., 2005), and thus we use the data reported in the DISS Working Group (2015) database.

In general, we determined the length and width of fault ruptures using the empirical relation of Wells and Coppersmith (1994) and used the inferred hypocentre as the fault centre, for both focal depths D^1 and D^2. By using this approach, we have obtained four stress change values for each source-receiver pair, which have been processed to obtain an average value and its associated standard deviation indicating the level of uncertainty.

In addition, for large earthquakes ($Mw > 6$) and for a focal depth $D^1 = 4.5$ km, considering that the fault top depth is above the topographic surface, D^1 has been adapted to fulfil the Wells and Coppersmith's (1994) criterion. This approximation also neglects the role of composite seismic sources (i.e., more ruptures of any size up to Mw_{MAX}; e.g., Pantosti and Valensise, 1990) that likely triggered some of the main seismic events of the Northern Apennines. Keeping in mind the above limitations, we nonetheless infer the static stress changes potentially produced by past earthquakes on the basis of available geological, structural and subsurface data. In some cases we have used the seismic sources reported in the DISS database (Basili et al., 2008; DISS Working Group, 2015), while in other cases we have considered minor or substantial differences with respect to the DISS catalogue, or we have proposed new seismic sources, such as for the Romagna and Mugello.

2.2. Fault-slip data collection

In the attempt to minimize the problems deriving from the ambiguity or the lack of data on the seismic sources, we have conducted a geological and structural study to address the kinematics and geometry of the potential source faults in the Northern Apennines. The obtained field data on active faults have been compared with those reported in recent databases of Italian seismic sources (ITHACA, Michetti et al., 2000; DISS Working Group, 2015; Basili et al., 2008). Specifically, various types of kinematic indicators (mechanic striations, shear veins, slickensides, etc.) have been collected on fault planes. In this analysis, we have distinguished fault-slip data collected on the master fault plane, in the fault core, and in the fault damage zone, which represents the volume of rocks containing subsidiary faults on either side of the fault core. We have also distinguished mesoscopic faults not clearly connected to a major fault, that may have clustered in deformation bands outside the damage zones (Table 1). The rake of a supposedly active fault (following the Aki and Richards' 1980 convention) has been determined through the statistical distribution of the measured fault slip vectors. It is worth noting that slip on single normal faults may vary depending on the position along the fault plane, with dip-slip and oblique-slip movements being dominant in the centre and the tips of the fault, respectively; the oblique-slip at the fault tips is typically directed toward the fault centre (e.g., Roberts and Michetti, 2004; Philippon et al., 2015). To minimize this kind of problems, we have primarily considered in our calculations the kinematics determined in the central part

Table 1
Fault-slip data collected from selected sites of measurement along the axial zone of the Northern Apennines. The terms 'master fault plane' and 'damage zone' refer respectively to the fault core and subsidiary faults in the fault damage zone, whereas the term 'mesoscopic faults' indicates brittle elements not clearly connected to a major fault (see text for details).

Site number	Locality	Coordinates		Kind of structure	Number of structures
		Lat N	Long E		
Valtiberina					
1	Il Carmine	43.5678	12.0242	Mesoscopic faults	3
2	San Leo	43.5289	12.0817	Damage zone	6
3	Fighille	43.5228	12.1011	Damage zone	7
4	Sansepolcro	43.5818	12.1367	Master fault plane	4
5	San Giustino	43.5550	12.1781	Damage zone	2
Romagna					
6	Premilcuore	43.9742	11.7674	Mesoscopic faults	11
7	Premilcuore	43.9706	11.7653	Mesoscopic faults	7
8	Cabelli	43.9291	11.8525	Mesoscopic faults	6
9	Cabelli	43.9316	11.8595	Mesoscopic faults	6
10	Gamberini	43.9044	11.9656	Master fault plane	6
11	Montegranelli	43.8807	11.9731	Damage zone	15
Mugello					
12	Brasimone	44.1222	11.1026	Master fault plane	16
13	Rasora	44.1151	11.1381	Damage zone	4
14	Mt. Altuzzo	44.0410	11.3849	Mesoscopic faults	8
15	Case di Risolaia	44.0258	11.4109	Damage zone	14
16	Santa Maria a Vezzano	43.9986	11.4600	Damage zone	17
17	Gattaia	43.9927	11.4754	Damage zone	4
Garfagnana					
18	Cerretoli	44.1073	10.3742	Damage zone	6
19	Careggine	44.1233	10.3324	Damage zone	12
20	Lake Vagli	44.1294	10.3047	Mesoscopic faults	12
21	Corfino	44.1803	10.3845	Master fault plane	7
Lunigiana					
22	Groppodalosio	44.4198	9.9472	Damage zone	5
23	Vignolo	44.3798	9.9805	Damage zone	9
24	Vignolo	44.3683	9.9718	Damage zone	11
25	Iera	44.3333	10.0406	Damage zone	9
26	Crocetta	44.3122	9.8508	Damage zone	7
27	Montereggio	44.2968	9.8379	Master fault plane	10
28	Villa (Tresana)	44.2534	9.8997	Master fault plane	8

of the fault. When data on active faults were not available in the Coulomb stress elaborations we have considered a rake of 90° and −90° for thrust and normal faults, respectively. In order to constrain the subsurface geometry of the causative faults, we have integrated the surface geological data with information from available seismic reflection profiles and instrumental seismicity recorded during specific seismic sequences (see below Section 2.3).

2.3. Earthquake location using dense seismic networks

The most recent seismic sequences that have occurred in Mugello (March 2008, $Mw_{MAX} = 4.5$; April 2009, $Mw_{MAX} \approx 4.2$) and in Romagna (July 2011, $Mw_{MAX} = 4.15$) have been recorded by dense seismic networks, giving us the opportunity to constrain the geometry of the causative active faults. Seismic measurements have been performed using Lennartz 3D/5s seismometers characterized by a sensitivity of 400 V/(m/s) and eigenperiod of 0.2 Hz. Seismic data have been recorded at 100 Hz using Guralp CMG-DM24 digitizers characterized by 24-bit resolution, and equipped by GPS for time synchronization. We recorded a total of 274 earthquakes with local magnitude ranging between 0.2 M_L and 4.2 M_L that have been located by manually picking the P-wave arrival times at all stations and by applying the least-square generalized inverse method (Lay and Wallace, 1995) considering a homogeneous half space. The uniform velocity model approximation can be considered valid since all stations are located within an epicentre distance range comparable with the earthquake depths. We assumed an average compressional wave velocity V_P of 7.2 km/s, calculated using a V_P/V_S ratio of 1.8 and an S wave velocity of 4 km/s (Piana Agostinetti et al., 2002). The error in the hypocentre location is <144 m, which has been calculated by considering the average misfit between predicted and measured times of P wave arrivals and the average compressional P-wave velocities.

3. Main seismic sources in the Northern Apennines

Seismic sources that have potentially generated past earthquakes in the Northern Apennines are described following the time–space progression of the main earthquakes during 1916–1921. In the following study, we start by describing the structures along the Pede-Apennine margin of Po Plain, and then we continue toward the axial zone, describing 6 key areas from southeast to northwest.

3.1. Pede-Apennine thrust and external thrust fronts

The Pede-Apennine margin is an important morphotectonic feature that separates the exposed thrust wedge on the southwest, from the topographically flat Po Plain on the northeast (Fig. 1a). The Pede-Apennine margin corresponds to a ~300 km-long system of NE-verging stacked thrust sheets, which is referred to hereinafter as Pede-Apennine thrust (Pieri and Groppi, 1981; Piccardi et al., 1997; Rossi et al., 2002; Bonini, 2013). Commercial seismic reflection profiles revealed the existence of well-developed systems of SSW-dipping blind thrust faults buried beneath the Po Plain deposits (Pieri and Groppi, 1981). The buried structures controlled the deposition of thick syntectonic sequences with maximum thickness of 7–8 km in the Pliocene-Quaternary infill (Pieri and Groppi, 1981; Barberi and Scandone, 1983; Fantoni and Franciosi, 2010). These structures exhibit arcuate traces in map view, and define the main Ferrara arc that represents the buried leading edge of the fold-and-thrust belt (Pieri and Groppi, 1981; Fig. 1a).

Earthquake fault plane solutions, macroseismic data of historical earthquakes and morphostructural investigations along the Pede-Apennine margin and in the Po Plain suggest that both frontal thrusts and lateral thrust ramps are active and potentially seismogenic (e.g., Piccardi et al., 1997; Benedetti et al., 2003; Boccaletti et al., 2004, 2011; Ciaccio and Chiarabba, 2002; Michetti et al., 2012; Burrato et al., 2003; Scrocca et al. 2007; Picotti et al., 2009; Gunderson et al., 2013; Vannoli et al., 2015a; Maesano et al., 2015) (details of focal mechanism solutions are given in Table S1). The recent seismic sequence of May 2012 (Mw_{MAX} 5.9 to 6.1 depending on the bibliographic source), nucleated on the western sector of the buried Ferrara arc thrust front, exemplifies the ongoing activity of this thrust system (e.g., Vannoli et al., 2015a). The last seismic event represents the highest earthquake magnitude recorded in this sector of the thrust belt. The highest macroseismic magnitude of historical seismic events along the Pede-Apennine margin approaches $Mw \approx 6$, such as for the earthquakes of 1501 ($Mw = 5.98$) and 1781 ($Mw = 5.94$) (Rovida et al., 2011). The 1781 Cagli earthquake ($Mw = 6.42$) is one of the strongest events, and struck an area located a few tens of kilometres southwest of the Pede-Apennine margin (Fig. 2a). This earthquake has been considered to have slipped along a deep thrust (Basili et al., 2008; DISS Working

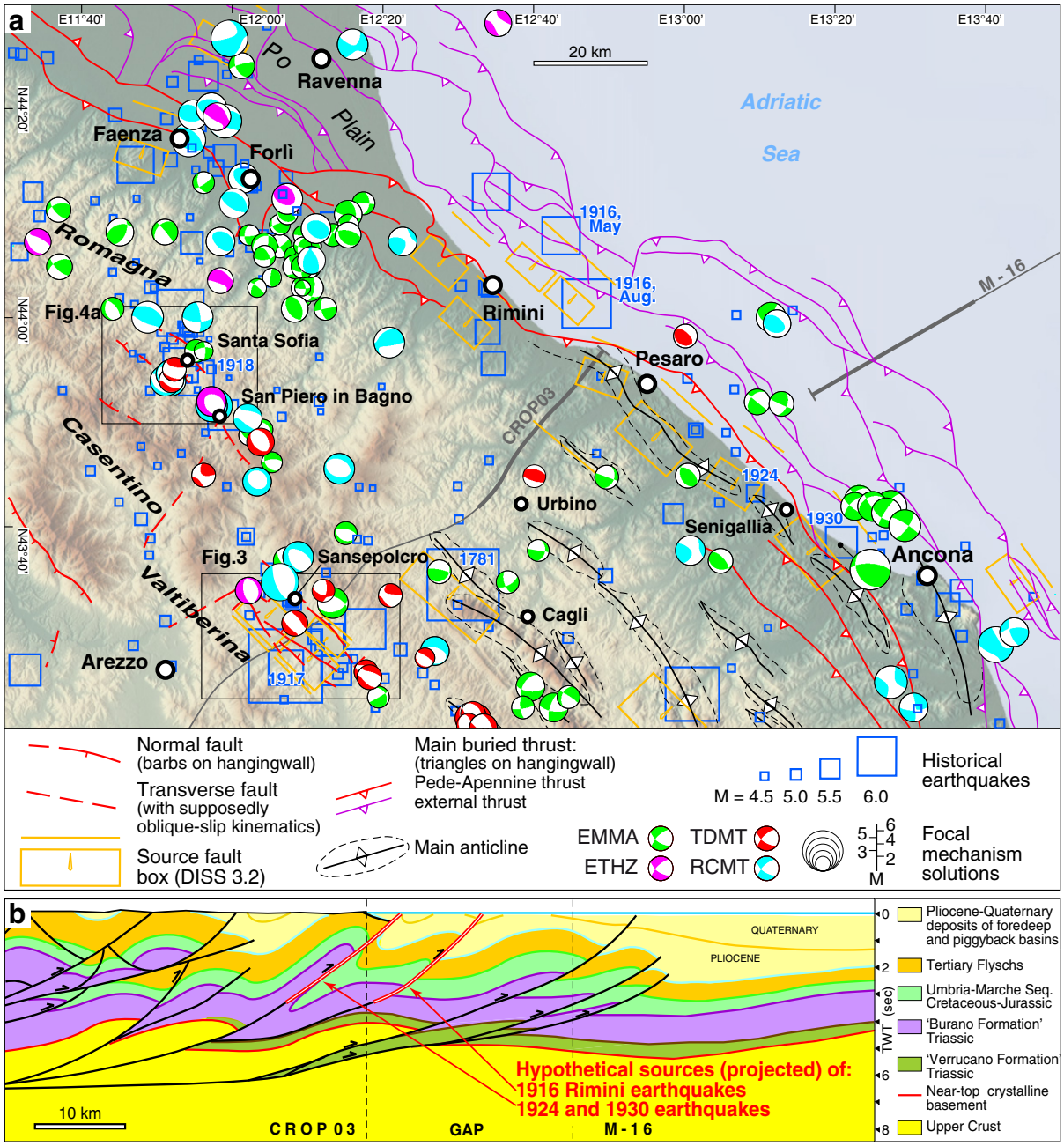

Fig. 2. (a) Main structural features of the junction area between the Pede-Apennine thrust and the external thrusts in the southeastern Po Plain, and in the adjacent sector of the axial zone including the Valtiberina and part of Romagna. The main structures are adapted from Barberi and Scandone (1983). Historical earthquakes are from the CPTI11 catalogue (Rovida et al., 2011). The focal mechanism solutions of earthquakes are reported from various sources (see Table S1 for details). The individual seismic sources are reported from Basili et al. (2008) and DISS Working Group (2015). (b) Interpreted seismic profiles CROP03 and M16 across the external thrust fronts (modified from Finetti et al., 2005); the considered parts of the seismic sections are shown as thick lines in the profile trace in panel (a). The inferred causative thrust faults of 1916, 1924 and 1930 earthquakes are indicated.

Group, 2015), an interpretation that is consistent with the presence of deep thrust earthquakes in the sector next to the axial extensional belt (Fig. 2a). Other authors instead are in favour of a genetic link of the Cagli earthquake with the low-angle extensional 'Altotiberina fault system' (Brozzetti et al., 2009).

A main seismic sequence hit offshore Rimini in 1916, with the seismic events that nucleated approximately in the area between the Pede-Apennine thrust and the more external buried thrusts (Fig. 2a). The 1916 sequence was characterized by the two main seismic shocks of May 17 (Mw = 5.94) and August 16 (Mw = 6.14). Many other seismic events with Mw ≤ 5.5 had hit the area the day before, the same day, and few days after the August 16 main shock. Other relevant earthquakes occurred south-eastwards along the same external thrust system, particularly the Mw = 5.36 Mondolfo earthquake of January 2, 1924 and the Mw = 5.81 Senigallia earthquake of October 30, 1930 (Basili et al., 2008; Rovida et al., 2011; Vannoli et al., 2015b) (Fig. 2a). The deep seismic profiles CROP03-M16 cut across this active thrust system south of Rimini, and the interpreted architecture of the structures may provide some hints for the construction of a geodynamic and seismotectonic model. More specifically, the CROP03-M16 profiles allow to image the frontal thrust system, forming the active leading edge of the chain (Finetti et al., 2001, 2005), which apparently has

produced the earthquakes of Rimini 1916, Mondolfo 1924 and Senigallia 1930 (Fig. 2b). The growth of coastal anticlines driven by blind-thrust faulting (Vannoli et al., 2004) and the deformation of the Adriatic Sea floor in correspondence of a thrust fault (Finetti et al., 2001) clearly point to an ongoing activity of the thrust front (Fig. 2a, b).

3.2. Valtiberina

The Valtiberina basin (or Upper Tiber basin; Fig. 3) hosts part of the upper course of the Tiber River, and is connected to the major Tiber basin that extends for more than 100 km to the south. Transverse faults segment this major basin, such as those that delimit the Valtiberina to the northwest (e.g., Bonini, 2009). The study of the region acknowledges an intense seismicity and historical earthquakes with high macroseismic magnitude, as exemplified by the events of 1352 (Mw = 6.44), 1389 (Mw = 5.99), 1458 (Mw = 5.78), 1789 (Mw = 5.84), and 1917 (Mw = 5.89) (Rovida et al., 2011) (Fig. 3). The seismic activity is predominantly related to an extensional domain (Ciaccio et al., 2006), and is most probably tied to the presence of active NW–SE-trending normal faults that bound both margins of the Valtiberina basin (Tanini, 1998; Delle Donne et al., 2007; Brozzetti et al., 2009; Barchi and Ciaccio, 2009; Sani et al., 2009). To be more specific, the Tiber River is flowing in a central depression that is bounded by two active normal fault systems, the SW-dipping 'Sansepolcro fault system' on the northeast and the NE-dipping 'Anghiari fault system' on the southwest (Figs. 3 and S1a). The latter is considered the basin master fault and is part of the regional low-angle Altotiberina fault system (Boncio et al., 2000; Barchi and Ciaccio, 2009; Brozzetti et al., 2009). Fault-slip data collected along the trace of active basin-bounding faults indicate an average dip-slip normal kinematics, with limited left-lateral component (average rake = −85°) (see stereonets 1–5 in Fig. 3; Table 1). The ongoing activity of these faults is suggested by their control on the drainage network as well as by the deformation and architecture of the late Pleistocene–Holocene deposits (Cattuto et al., 1995; Delle

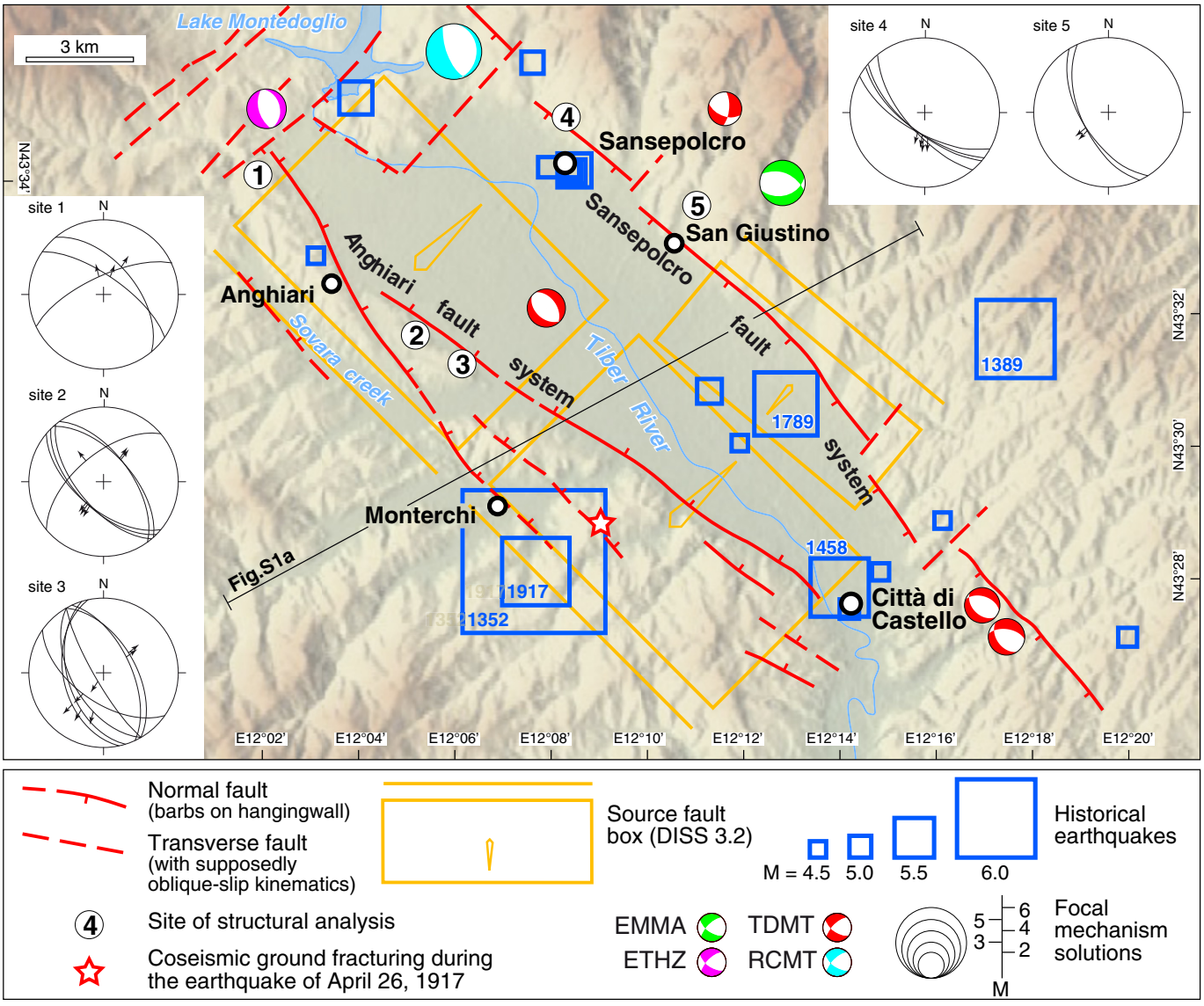

Fig. 3. Main structural features of the Valtiberina area (location in Fig. 2a). The active faults are compiled from various sources (Tanini, 1998; Michetti et al., 2000; Delle Donne et al., 2007; Bonini, 2009; Sani et al., 2009; DISS Working Group, 2015). The stereonets illustrate the fault-slip data collected at structural stations (cyclographic lines; Schmidt net, lower hemisphere) (from Tanini, 1998). Historical earthquakes are from the CPTI11 catalogue (Rovida et al., 2011). The focal mechanism solutions of earthquakes are reported from various sources (see Table S1 for details). The individual seismic sources are reported from Basili et al. (2008) and DISS Working Group (2015). The location of the coseismic ground fractures that appeared during the April 26, 1917 earthquake is reported from Oddone (1918).

Donne et al., 2007; Sani et al., 2009). The most relevant indications of active faulting have been identified on the NE-dipping normal faults on the southwestern basin margin; here the displacement of stratigraphic markers and syntectonic sedimentary wedging of Middle Pleistocene–Holocene deposits on the fault hangingwall are imaged through high-resolution shallow seismic profiles and well logs (Delle Donne et al., 2007; Sani et al., 2009). The seismic line interpretation suggests that the Anghiari fault on the southwestern margin dips ~50° to the northeast (cf. Barchi and Ciaccio, 2009; Brozzetti et al., 2009; Sani et al., 2009), and is characterized by an average slip-rate of ~0.25 mm/year (Delle Donne et al., 2007).

In agreement with the DISS Working Group (2015) catalogue, we therefore consider the NE-dipping Anghiari fault system as the most probable seismogenic source of the 1917 earthquake (e.g., Sani et al.,

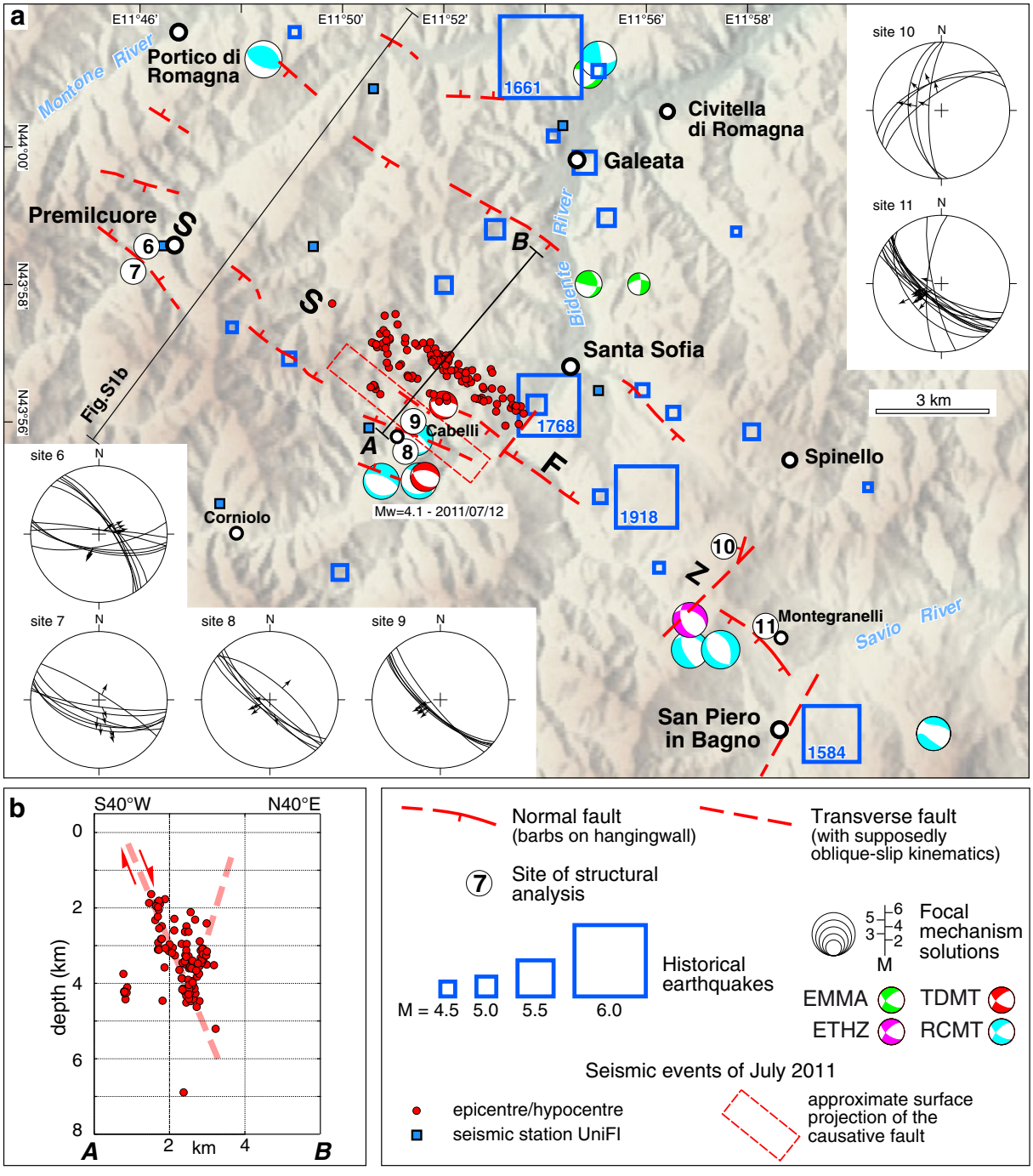

Fig. 4. (a) Main structural features around Santa Sofia, in Romagna (location in Fig. 2a). SSFZ, Santa Sofia fault zone. The stereonets illustrate the outcrop-scale faults collected at structural stations (cyclographic lines; Schmidt net, lower hemisphere). Historical earthquakes are from the CPTI11 catalogue (Rovida et al., 2011). The focal mechanism solutions of earthquakes are reported from various sources (see Table S1 for details). The earthquakes that followed the seismic shock of July 12, 2011 were monitored through the installation of a local seismic network (seismic stations of the University of Firenze, UniFI), and the position of these events is indicated (small red circles). (b) Hypocentres of the seismic events that followed the July 12, 2011 seismic shock. The depth distribution of these seismic events defines a steep (~65°) NNE-dipping seismogenic normal fault, and possibly a secondary antithetic normal fault (thick red dashed lines); the trace of profile AB is reported in panel (a).

2009) (Fig. 3). Macroseismic evidence shows indeed that the highest damaged area associated with this earthquake occurred on the southwestern basin margin and suggests a NW–SE orientation of the causative fault (Valensise and Pantosti, 2001). Interestingly, Oddone (1918) reported the presence of some NW–SE-trending co-seismic fissures that formed near Monterchi during the 1917 earthquake (Fig. 3). In particular, this fissure system displayed vertical ground displacement (~25 cm), and localized into a 6 m-wide, 1 km-long belt situated approximately along the surface trace of NE-dipping normal faults on the southwestern basin margin (Fig. 3). The above information hints therefore that the NE-dipping Anghiari fault system is to be considered the seismogenic source that ruptured during the 1917 earthquake.

3.3. Santa Sofia in Romagna

The Romagna region (Fig. 4a) is characterized by historical earthquakes with notable macroseismic magnitude, namely: 1584 (Mw = 5.80), 1661 (Mw = 6.09), 1768 (Mw = 5.87), and 1918 (Mw = 5.88) (Rovida et al., 2011) (Fig. 4a). However geological and morphostructural evidence of active structures are scarce in the area. According to previous geological-structural studies (Benini and Farabegoli, 1991), the 1918 Santa Sofia earthquake has been attributed to a NNE-striking sinistral transpressional fault system running approximately along the Bidente valley (Mantovani et al., 2009; Viti et al., 2012). Landuzzi (1991) referred instead the neo-tectonic activity in the sector to ~NW–SE-trending normal faults. In the field survey, we have identified further significant ~NW–SE-trending normal faults between Santa Sofia and San Piero in Bagno (Fig. 4a, Table 1). These normal faults outline an extensional zone, referred to herein as 'Santa Sofia fault zone' (SSFZ), which is located northeast of the main watershed.

A local seismic network was installed south of Santa Sofia just after this area was hit by five small-to-moderate seismic shocks (Mw_{MAX} = 4.15) on July 12, 2011 (Fig. 4a, Table S1). The seismic recording lasted 5 days from July 14 to July 18, 2011 and was conducted using seven broadband seismic stations specially deployed within an area of 5 km radius centred on the main-shock epicentre (Fig. 4a). These recordings provided a dataset consisting of 145 aftershocks with local magnitude ranging between 0.5 and 3.1 M_L.

In plain view, the recorded epicentres cluster along a NW–SE-trending alignment that is sub-parallel to the SSFZ (Fig. 4a). The microseismic events extend up to ~7 km depth, but concentrate essentially in the 2–5 km depth range; the depth distribution of these events allows the identification of a normal fault dipping ~65° toward north-northeast (Fig. 4b). This fault is not associated with a distinctive surface fault scarp, but instead we have surveyed several outcrop-scale NNE- and SSW-dipping normal faults with small vertical throw along the SSFZ, which encompass the surface projection of the 2011 seismogenic fault (Fig. 4a). This suggests that the seismogenic structure is only partially outcropping, and the minor faults would mostly represent splays of the main normal fault, or accommodate the surface extensional deformation in the form of antithetic structures that may mimic the hangingwall fall during normal faulting (e.g., Doglioni et al., 2014) (Figs. 4a, b and Fig. S1b). Fault-slip data collected on these minor faults indicate a dominant dip-slip kinematics with slight dextral components (see stereonets 6–11 in Fig. 4a), which we also assume to be valid for the main fault segment (average rake = −95°).

The microseismic events of 2011 illuminate a ~4.5 km-long fault segment, whereas the outcrop-scale normal faults occur over a belt extending for a length of more than 15 km to the southeast of the 2011 events. Notably, the macroseismic epicentres of three important historical earthquakes (i.e., the events of 1584, 1768, and 1918) are aligned along this belt (Fig. 4a). Two recent earthquakes (Mw_{MAX} = 4.7) with extensional focal solution and shallow focal depth (≤10 km) hit the south-eastern sector of the SSFZ on January 26, 2003 (Piccinini et al., 2009; Fig. 4a). The group of associated microearthquakes defines a broad SW-dipping fault plane (Piccinini et al., 2009), which is compatible with the presence of the nearby SW-dipping normal fault (Montegranelli area; Fig. 4a). Another extensional seismic event with similar characteristics (Mw ≈ 4, focal depth ~ 8 km) occurred on July 11, 2013 ~ 6 km southeast of San Piero in Bagno (see Fig. 2a and Table S1).

The spatial distribution of the minor normal faults and the associated morphologic features seemingly reflect the trace of the main fault, whose length would be compatible with that of the ruptures produced by the historical earthquakes (with magnitude up to ~6). On this basis, we suggest that the NNE-dipping normal fault may represent a possible, shallow (≤10 km) seismic source for some of the Mw ≈ 6 Romagna earthquakes. The attribution of the Mw ≈ 6.1 1661 earthquake, whose epicentre is located more to the northeast with respect to the SSFZ appears to be more dubious (Fig. 4a). If the position of the 1661 earthquake is correct, we should also consider the possibility that this event was linked to the thrusting connected with the Pede-Apennine margin (see Fig. 2). Compressive seismic events with deep focal depth (20–30 km depth range) may indeed occur in this area, such as the Mw = 4.3 event of April 16, 2006 (focal depth ~25–27 km) whose epicentre is situated only 5 km southwest from the one of 1661 (Fig. 4a; Table S1).

3.4. Mugello

The Mugello sector (Fig. 5a) is characterized by a rather high seismicity with historical earthquakes having the highest macroseismic magnitude of Mw = 5.94 (1542) and Mw = 6.29 (1919) (Rovida et al., 2011). The main feature is the intramontane continental Mugello basin that is inferred to have developed in Late Pliocene–Early Pleistocene under a compressive regime and was later affected by normal faults as the compressive regime ceased around the Early-Middle Pleistocene transition (Sani et al., 2009). A large SSW-dipping normal fault system, referred to as 'Ronta fault system', affects the pre-basin substratum mostly made of Miocene sandstones, and delimits the north-eastern basin margin (Sani et al., 2009; Figs. 5a and S1c). This fault systems is ~25–30 km long and displays a remarkable morphostructural evidence (Fig. 6a). An average long-term vertical slip-rate of 0.16 to 0.37 mm/year has been estimated along the Ronta fault system (Sani et al., 2009). Fault-slip data indicate dip-slip normal kinematics with a minor left-lateral component (average rake = −85°; stereonets 15–17) (Figs. 5a and 6b, Table 1). A system of NE-dipping antithetic normal faults bounds the southwestern margin of the basin (Benvenuti and Papini, 1997; Sani et al., 2009) (Fig. 5a). This fault system is believed to control the asymmetric location of the Sieve River on this side of the basin (Benvenuti and Papini, 1997), even though the morphologic expression of these faults is scarcely pronounced. Previous studies have interpreted this fault system as the basin master fault (Martini and Sagri, 1993), which would be connected to the regional NE-dipping low-angle Etrurian normal fault system (Boncio et al., 2000). The DISS Working Group (2015) catalogue follows this model and subdivides the southwestern basin margin into a north-western and south-eastern fault segments, which are inferred to have caused the earthquakes of 1542 and 1919, respectively (Basili et al., 2008) (Fig. 5a). Transverse faults at the north-western and south-eastern basin margins are inferred to represent other potentially active structures (Delle Donne, 2005).

The installation of local seismic networks has allowed the recognition of another seismic structure on the north-western Mugello basin margin (Amato et al., 2008; Ripepe et al., 2008). The networks were installed after three small-to moderate seismic shocks (Mw_{MAX} = 4.5) struck this sector on March 1, 2008, with a hypocentral depth of ca. 12 km being (TDMT, Time Domain Moment Tensor; Scognamiglio et al., 2009). The recorded microseismic events occur in a 2–16 km depth range, are well clustered, and outline a steep normal fault dipping (~75°) toward the NNE (Amato et al., 2008; Ripepe et al., 2008)

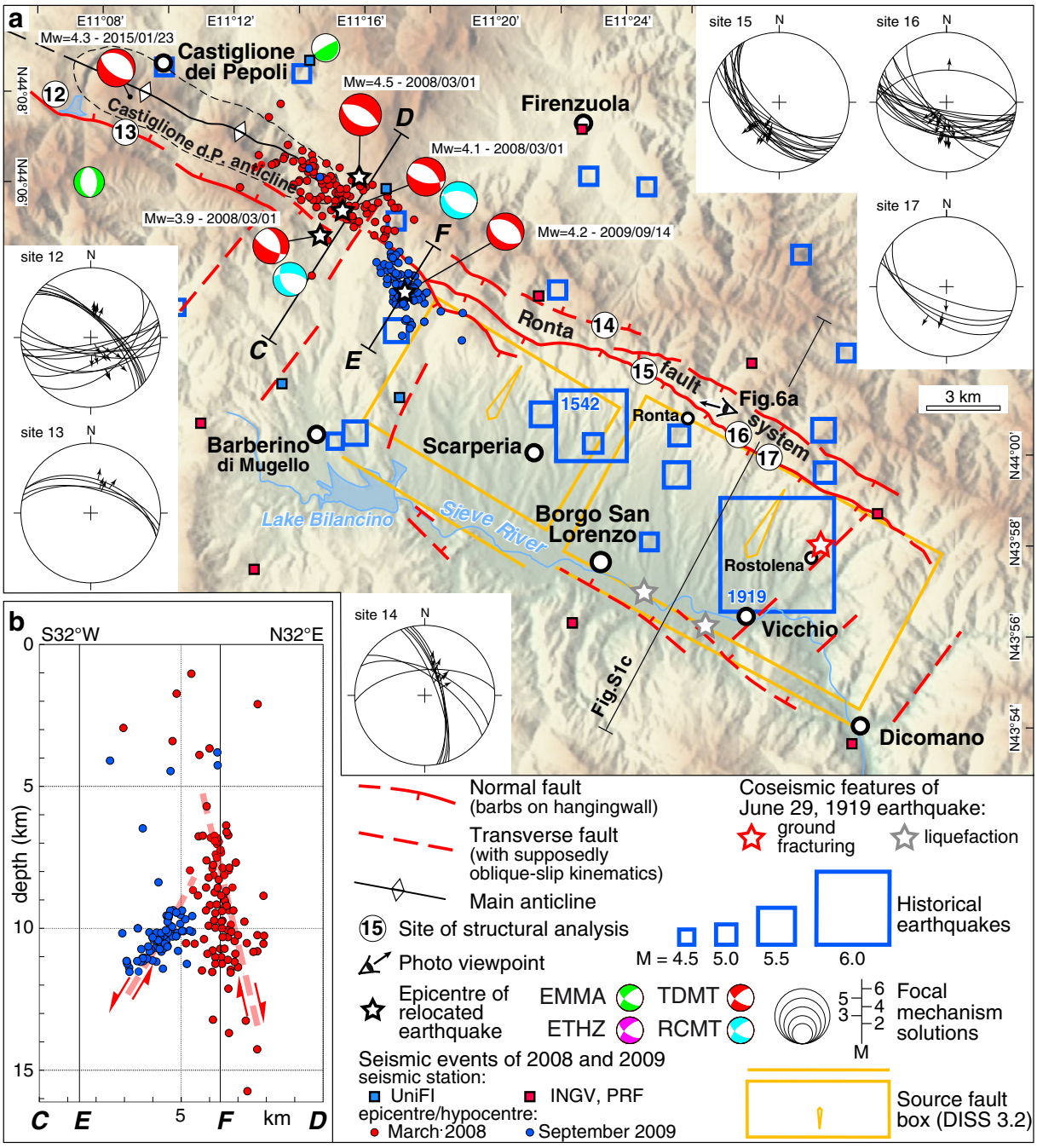

Fig. 5. (a) Main structural features of the Mugello area (location in Fig. 1a). The active faults are compiled from various sources (Delle Donne, 2005; Sani et al., 2009) and additional field surveys. The location of the coseismic ground fractures and liquefaction phenomena that appeared during the June 29, 1919 earthquake are reported from Capacci (1920) and Galli and Meloni (1993), respectively. The stereonets illustrate the fault-slip data collected at structural stations (cyclographic lines; Schmidt net, lower hemisphere). Historical earthquakes are from the CPTI11 catalogue (Rovida et al., 2011). The focal mechanism solutions of earthquakes are reported from various sources (see Table S2 for details) and Amato et al. (2008). The individual seismic sources are reported from Basili et al. (2008) and DISS Working Group (2015). The earthquakes that followed the seismic shocks of March 1, 2008 and September 14, 2009 were positioned through local seismic networks (Amato et al., 2008, Ripepe et al., 2008, and seismic bulletin of Prato Ricerche, downloaded at http://www.pratoricerche.it/). The main shocks of 2008 and 2009 have been manually relocated (Amato et al., 2008, and seismic bulletin of Prato Ricerche). Seismic station: UniFI, University of Firenze; INGV, Istituto Nazionale di Geofisica e Vulcanologia; PRF, Prato Ricerche Foundation. (b) Hypocentres of the seismic events that followed the main earthquakes of March 1, 2008 (after Amato et al., 2008 and Ripepe et al., 2008) and September 14, 2009 (seismic bulletin of Prato Ricerche). The depth distribution of the 2008 seismic events defines a steep NNE-dipping seismogenic normal fault, while the 2009 earthquakes identify a SSW-dipping normal fault of the Ronta fault system. The two interpreted faults (thick red dashed lines) are likely to interfere with each other. Note however that the geometry of the two faults shown in panel (b) cannot be used to infer their superposition relationships for the reason that the two series of earthquakes have been projected from different profiles located nearly 4 km apart (i.e., profiles CD and EF, whose trace is reported in panel a).

(Fig. 5b). The surface projection of this fault occurs a few kilometres northeast of the Ronta fault system, approximately along the ridge forming the main watershed. Previous structural analysis has highlighted a minor extensional deformation consistent with the kinematics and geometry detected for this NNE-dipping fault (Bonini, 2013). The field survey conducted for the current study has revealed the existence of other minor NNE-dipping fault scarps (stereonets 12–14), in which the extensional deformation may be occasionally accommodated by the reactivation of existing joints (stereonet 14; Fig. 5a). This fault could have generated the recent sequence of January 2015

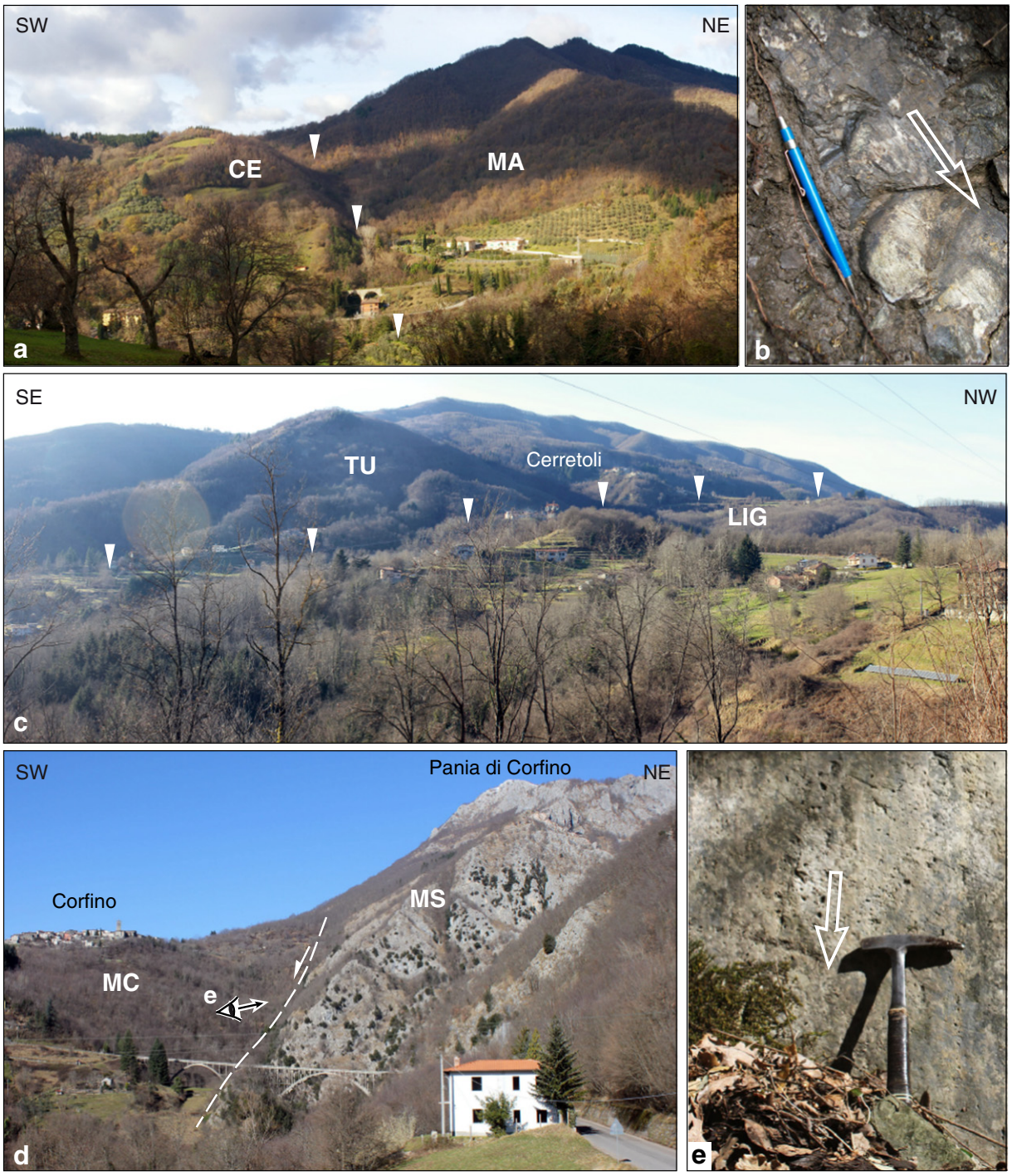

Fig. 6. Morphological evidence of some normal faults in the axial zone of the Northern Apennines. (a) Lateral view of the main SW-dipping Ronta normal fault (indicated by the tips of white triangles) in Mugello (north of Ronta; location in Fig. 5a). The normal fault is likely to reactivate the SW-dipping thrust carrying the Early Miocene Cervarola sandstones s.l. (CE) over the Middle Miocene Marnoso Arenacea sandstones (MA). (b) Slickensides on a shear plane near to the master fault plane of the Ronta normal fault; the open arrow indicates the movement of the missing block (site 15). (c) View of the main NE-dipping fault of the Careggine fault system in Garfagnana (location in Fig. 7a). The fault exposes rocks of the Late Triassic–Late Oligocene Tuscan Unit (TU) on the footwall and downfaults the tectonically overlying Late Cretaceous Ligurian Units s.l. (LIG), over which the Villafranchian continental deposits unconformably lie. (d) Lateral view and interpretative tectonic sketch of the SW-dipping Corfino normal fault in Garfagnana (location in Fig. 7a); MS, Mesozoic Massiccio limestone; MC, Tertiary Macigno sandstones. (e) Detail of striations on the Corfino master fault plane (site 21).

($Mw_{MAX} \approx 4.3$; TDMT), and also some moderate historical earthquakes ($Mw_{MAX} \approx 4.8$; Rovida et al., 2011) whose macroseismic epicentres fall on the watershed ridge northeast of the Mugello depression (Fig. 5a). A further seismic sequence ($Mw_{MAX} \approx 4.2$; TDMT) hit the Mugello depression on September 14, 2009. The local seismic network belonging to the Prato Ricerche Foundation (formerly Istituto Geofisico Toscano) allowed one to locate several aftershocks (Piccinini et al., 2014; see seismic bulletin of Prato Ricerche, downloaded at http://www.pratoricerche.it/), whose depth distribution defines a SSW-dipping normal fault referable to the Ronta fault system (Fig. 5a, b).

From these observations, it appears that there is a number of seismic sources that may potentiality produce earthquakes in the Mugello area. Coseismic rupturing of the ground surface by east–west-trending fractures was observed in the central-eastern part of the Mugello

depression (Villa Ricci, near Rostolena) during the seismic event of 1919 (Capacci, 1920), and liquefaction phenomena are reported nearby the Sieve river (Galli and Meloni, 1993) (Fig. 5a). Unfortunately, the location of these deformation features does not allow one to properly identify the source fault of that earthquake, which may be composed by more than one structure that could have ruptured during the event. Specifically, the distribution of the sites with highest damage may suggest that a transverse fault may have also been activated by the 1919 event (Delle Donne, 2005; Sani et al., 2009).

On the basis of length, lateral continuity, and its clear morphological evidence, we consider the Ronta fault system as the most likely source of the biggest earthquakes that hit the Mugello area, including the 1919 event. This interpretation is strengthen by the presence of historical and recent seismicity on the northeastern basin margin, particularly the 2009 events connected with the slippage along the Ronta fault system (Fig. 5a and Table S2). The distribution of the 2009 epicenters delineates a NW-trending belt that is remarkably parallel to the Ronta fault system. More specifically, the 2009 sequence localized near the northwestern tip of the SSW-dipping Ronta fault system, where a minor transverse fault system seemingly separates the latter from the splays connected to the steep NNE-dipping fault (Fig. 5a, b).

3.5. Garfagnana

The Garfagnana region (Fig. 7) is characterized by important seismic activity represented by several moderate-to-strong historical seismic

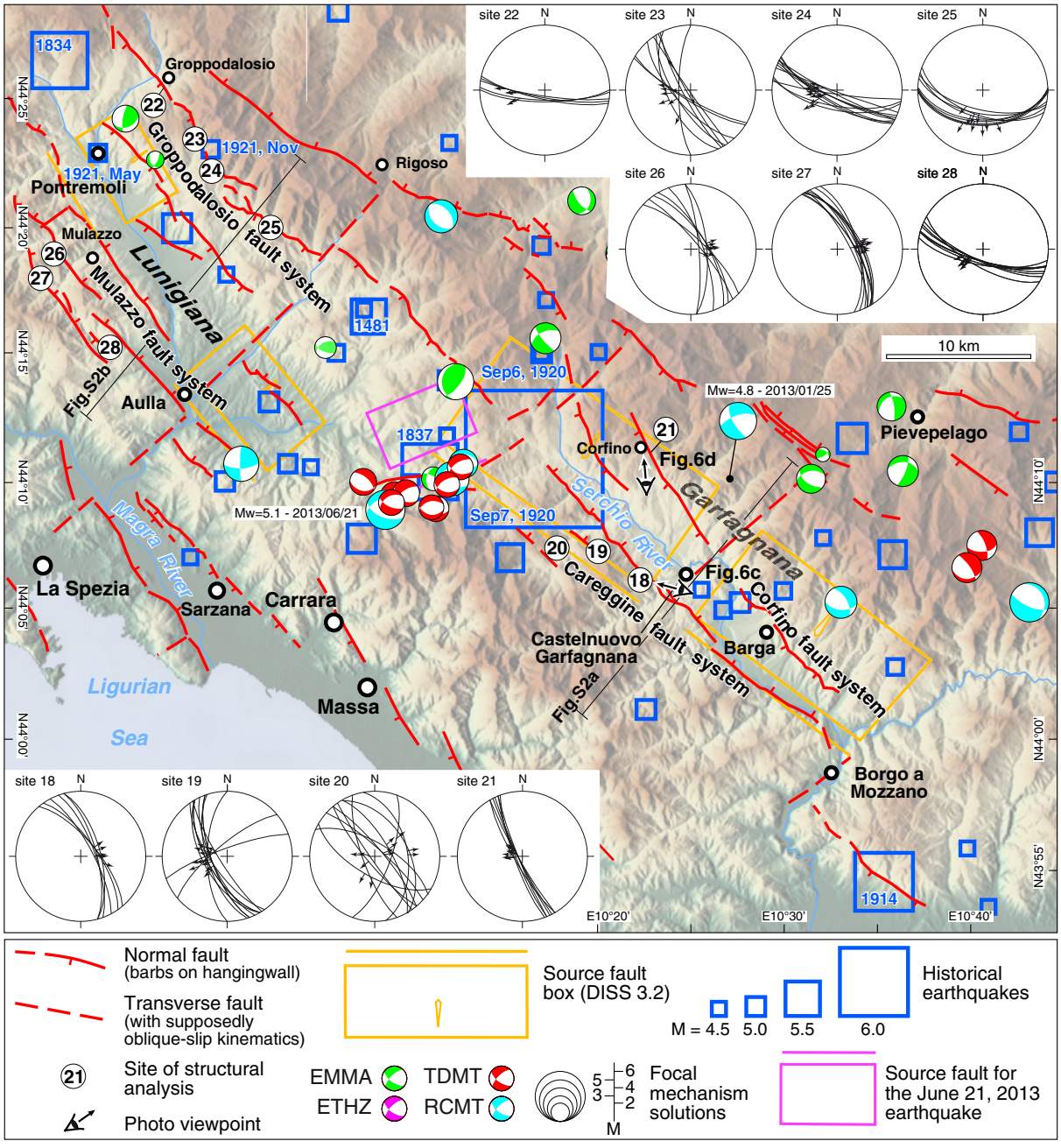

Fig. 7. Main structural features in the Garfagnana-Lunigiana sector (location in Fig. 1a). The active faults are compiled from various sources (Corti et al., 2006; Di Naccio et al., 2013) and additional field surveys. The stereonets illustrate the fault-slip data collected at the structural stations (cyclographic lines; Schmidt net, lower hemisphere). Historical earthquakes are from the CPTI11 catalogue (Rovida et al., 2011). The focal mechanism solutions of earthquakes are reported from various sources (see Table S3 for details). The individual seismic sources are reported from Basili et al. (2008) and DISS Working Group (2015). The source fault for the June 21, 2013 earthquake is from Stramondo et al. (2014).

events, particularly the Mw = 5.81 event of 1837 and the Mw = 6.48 (Rovida et al., 2011) and Ms = 6.48 (Margottini et al., 1993) earthquake of September 7, 1920, which is one of the strongest in the Northern Apennines. The Garfagnana area is characterized by a tectonic depression bounded on both margins by two oppositely-dipping NW-SE-trending fault systems and, for this reason, it is commonly referred to as the Serchio graben (e.g., Dallan and Nardi, 1974) (Figs. 7 and S2a). The normal faults bordering the Serchio graben were proven to be active during the late Quaternary (Bartolini et al., 1982). Recent geomorphic analysis of the fluvial network confirms the recent activity and the potentially seismogenic character of these faults (Di Naccio et al., 2013).

Calistri (1974) assumed the NE-dipping fault system being the master fault, based on the dominant SW-directed tilting of the basin deposits, while Eva et al. (1978) considered the SW-dipping fault system as the most important one. More recently, the master fault has been identified with the NE-dipping fault system bounding the southwestern basin margin, referred to herein as 'Careggine fault system', which is inferred to represent a sector of the regional Etrurian fault system (Boncio et al., 2000). The NE-dipping faults on the southwestern basin margin are characterized by strong morphologic evidence (Di Naccio et al., 2013) (Fig. 6c), and two NE-dipping fault segments have been identified as the main seismogenic structures, the north-western fault being recognized as the causative source of the Mw ≈ 6.5 earthquake of 1920 (Basili et al., 2008; DISS Working Group, 2015). Fault-slip data collected along the master fault planes indicate an essentially dip-slip kinematics of the normal faults (average rake = −95°) (stereonets 18–20; Fig. 7, Table 1).

The SW-dipping high-angle normal faults on the north-eastern basin margin, referred to herein as 'Corfino fault system', also show a very clear morphologic signature that hints to its recent activity (e.g., Di Naccio et al., 2013) (Fig. 6d, Table 1). Striations on the master fault plane indicate dominant dip-slip kinematics with minor dextral component of movement (average rake = −95°) (site 21; Fig. 6e). Two of the three sites with the highest MCS Intensity produced by the 1920 seismic event (I_{MAX} = X MCS; Rovida et al., 2011) are close to the trace of the Corfino fault system. This raises the possibility that this system was activated during the 1920 earthquake, or simply that the highest amplification was localized on the north-eastern basin margin. In the present study, we basically follow the DISS source fault model and assume the NE-dipping Careggine fault system as the causative source of the seismic event of 1920. Solarino (2005) estimated a focal depth of 4.5 km for the Mw ≈ 6.5 1920 earthquake; in our analysis we have used a focal depth of 6.5 km, based on the Wells and Coppersmith's (1994) relationships.

NE-ENE-trending transverse fault zones break the lateral continuity of the main graben-bounding faults (e.g., Molli et al., 2016). One of these structures delimits the Garfagnana graben to the northwest, whereas the other is internal to the graben (Fig. 7). In 2013 two moderate earthquakes nucleated on these transverse fault zones, particularly the Mw ≈ 4.8 and Mw ≈ 5.1 seismic events of January 25 and June 21, respectively (Fig 7 and Table S3). The macroseismic epicentre of the Mw ≈ 5.1 earthquake of September 6, 1920 – which hit the day before the large M ≈ 6.5 earthquake – is roughly located on the transverse fault zone that ruptured on June 21, 2013 (Fig. 7). For this reason, in further elaborations (see below Section 4.2) we have arbitrarily assumed that the source parameters determined by Stramondo et al. (2014) for the June 21, 2013 earthquake are also valid for the seismic event of September 6, 1920. Another transverse fault zone is likely to run along the Serchio valley that delimits the Garfagnana graben to the southeast (Fig. 7). Such a transverse structure seemingly transfers displacement on the ~10 km-long SW-dipping normal fault south-southeast of Borgo a Mozzano (cf. Bartolini et al., 1982). The macroseismic epicentre of the Mw ≈ 5.8 earthquake of October 27, 1914, for which Solarino (2005) has estimated a focal depth of 4.5 km, is almost coinciding with the trace of this normal fault, therefore we speculatively assume that the latter was the causative source (Fig. 7).

3.6. Lunigiana

The Lunigiana area (Fig. 7) is characterized by a significant historical seismicity, particularly the Mw = 5.55 and Mw = 5.83 events of 1481 and 1834 (Rovida et al., 2011). Similarly to the Garfagnana one, the Lunigiana area hosts a graben bounded by oppositely-dipping normal faults with Quaternary activity (Bartolini et al., 1982). The most important graben-bounding fault systems are referred to as 'Groppodalosio' and 'Mulazzo' on the north-eastern and south-western margins respectively (Bernini and Lasagna, 1988; Bernini and Papani, 2002) (Figs. 7 and S2b). Bernini and Lasagna (1988) considered the Groppodalosio fault system as the basin master fault. More recently, the Mulazzo fault system has been determined to accommodate more than 2500 m of vertical displacement, while the vertical throw across the Groppodalosio fault system may reach ~2000 m, therefore identifying the basin master faults as those on the southwestern margin (Artoni et al., 1992; Bernini and Papani, 2002). Accordingly, Boncio et al. (2000) have considered this normal fault system as the surfacing of the regional NE-dipping Etrurian fault system. A similar geometry has been inferred on the basis of the interpretation of a regional seismic profile linking the Lunigiana graben to a NE-dipping extensional detachment (Argnani et al., 2003). This setting is also consistent with the distribution of the seismicity that from the Lunigiana graben deepens (~30°) to the northeast, parallel to the basement top (Eva et al., 2014). The mechanical connection of the low-angle detachment with the external thrusts may be problematic, but this issue is beyond the purpose of the present study.

The Mulazzo and Groppodalosio systems are arranged en-echelon and are characterized by fresh morphostructural features (Piccardi et al., 1999), and relationships with the drainage network point to recent and ongoing fault activity (Di Naccio et al., 2013). The DISS database considers the main seismogenic sources of Lunigiana to be represented by two NE-dipping fault segments on the southwestern basin margin, the north-western fault segment (next to Pontremoli) being identified as the causative source for the Mw ≈ 5.8 earthquake of 1834, and the south-eastern fault segment (beside Aulla) for the Mw ≈ 5.5 seismic event of 1481 (see Fig. 7a; Basili et al., 2008; DISS Working Group, 2015). Basically, we assume the DISS source fault model, and attribute an average rake of −100° to the Mulazzo fault system, based on the surveyed fault kinematics (stereonets 26–28; Fig. 7, Table 1). Fault-slip data collected along the master fault planes of the Groppodalosio system indicate a dip-slip kinematics with a minor, but systematic, dextral component of the normal faulting (average rake = −105°) (stereonets 22–25; Fig. 7, Table 1). This fault kinematics matches well with the fault-slip data reported in Bernini and Lasagna (1988) for the Groppodalosio fault system.

The Mw ≈ 4.7 and Mw ≈ 4.6 seismic events of May and November 1921 followed the large Garfagnana earthquake of September 1920, and closed the north-western propagation of the normal fault seismicity. Based on the distribution of the macroseismic epicentres and the macroseismic intensity (Rovida et al., 2011) it is suggested that the first and the second events occurred respectively on the Mulazzo and Groppodalosio fault systems.

4. Evaluation of Coulomb stress changes

4.1. Idealized stress transfer interaction among seismic sources

We investigated the elastic stress interaction between seismic sources along the external thrust fronts and the axial seismogenic belt under the assumption that small Coulomb stress changes can promote earthquakes when the faults are close to failure. The thrusts forming the external Adriatic fronts show a trend roughly similar to that of the normal faults in the axial zone. In particular, the historical datasets suggest that the belt of seismogenic normal faults and the Pede-Apennine thrust have the potential to create earthquakes with magnitude up to

~6.5 and ~6.1. We explore the conditions under which earthquakes on the thrust and normal fault systems can promote failure on surrounding faults of the same system, as well as how one system can influence the other. We thus analyse a series of faulting configurations between source (SF) and receiver (RF) faults representative of the study area. In the present analysis we do not consider the deep and strong thrust earthquakes hypothesised to nucleate close to the axial extensional belt (i.e., the 1781Mw ≈ 6.4 Cagli earthquake; see Section 3.1).

We took into consideration two main cases, specifically when the source fault is (1) an external thrust segment or (2) an axial normal fault. In the first case, the simplest condition happens with a planar source thrust and a normal fault dipping either (a) parallel (synthetic) or (b) oppositely (antithetic) to the thrust. The Coulomb stress changes produced by an external thrust segment load both synthetic and antithetic distal normal faults, with the stress change magnitude evidently increasing with the decreasing distance between the source and the receiver (Fig. 8a, b). In particular, a hypothetical Mw = 6.1 rupture along the Pede-Apennine thrust may produce stress changes up to ~0.15–0.2 bar at a distance of 35–40 km, which is the minimum distance between the Pede-Apennine thrust and the axial normal faults. In another case we considered adjacent thrust faults, the thrust fronts being composed of several adjacent along-strike segments (Fig. 8c). An along-strike receiver thrust is brought closer to failure by the contiguous source thrust, but the stress decays rapidly at distances greater than about one rupture width (Lin et al., 2011). In particular, the stress changes are raised mainly on the half part of the receiver close to the rupture (Fig. 8c).

The second case we considered regards the stress changes caused by an Mw = 6.5 normal-fault earthquake on receiver distal thrusts dipping either (d) parallel or (e) oppositely to the source fault (Fig. 8d, e). A Mw = 6.5 rupture can produce a positive Coulomb stress change on a receiver thrust dipping both parallel and oppositely to the source. The configuration with parallel source and receiver faults is however more favourable for transmitting stresses (cf. Fig. 8d and Fig. 8e).

Finally, we consider the effects of a Mw = 6.5 normal fault rupture on adjacent and parallel along-strike or an-echelon normal faults (Fig. 8f). The distance between normal fault segments is variable in that in-basin normal faults are close whereas faults may occur at few tens of kilometres away in an-echelon basins. In the considered case, the Coulomb stress changes are raised on both the adjacent and an-echelon receiver fault, but with higher magnitude in the former case (Fig. 8f). In these conditions the stress falls off less rapidly than in the case of adjacent thrust segments — i.e., the stress propagates much beyond one source width (cf. Fig. 8c and Fig. 8f). The results also suggest

Table 2
Seismic source parameters of the main earthquakes (bold) of the time–space cluster of seismic events that hit the Northern Apennines in the period 1916–1920. The list also includes: (i) selected moderate earthquakes (Mw ≥ 5 ± 0.25) that struck the study region in the period 1900–1915, before the onset of the 1916–1920 seismic cluster, (ii) the large Avezzano earthquake of 1915, and (iii) the moderate events of Lunigiana in 1921 (see also Fig. 1a). The Coulomb stress changes (ΔCFF) are calculated at the lower and upper boundaries of a seismogenic layer defined by an upper boundary D^1, fixed at 4.5 km depth (based on Solarino (2005)), and a lower boundary D^2 calculated from the 75% of seismicity cutoff (e.g., Chiarabba et al., 2005). Fault parameters (including depth) for the more external thrust faults are taken from DISS Working Group (2015). The cumulative Coulomb stress changes (ΔCFF_{cum}) for a given earthquake are reported as a range of minimum and maximum values obtained from Eq. (3) using the mean and standard deviation associated with each source-receiver pair. The values are relative to cumulative ΔCFF_{cum} loading each structure over two different time windows (1900–1915 and 1916–1921). The ΔCFF value loading each receiving structure by each earthquake is reported in Table S4.

Locality	Earthquake	Mw	Lat N	Long E	Causative/receiver fault					Cumulative ΔCFF_{cum} (bar)	
					Strike (deg)	Dip (deg)	Rake (deg)	Depth (km)		1900–1915	1916–1921
								D^1	D^2		
Garfagnana	1902 03 05	4.96[a]	44.093[a]	10.463[a]	320[b]	60[b]	−95[b]	4.5[b]	10.5[b]		
Garfagnana	1902 08 04	5.14[a]	44.200[a]	10.200[a]	320[b]	60[b]	−95[b]	4.5[b]	10.3[b]		
Lunigiana	1903 07 27	5.25[a]	44.329[a]	9.953[a]	330[b]	60[b]	−100[b]	4.5[b]	10.0[b]		
Reggiano	1904 02 25	5.05[a]	44.490[a]	10.640[a]	115[b]	35[b]	90[b]	4.5[b]	28.6[b]		
Frignano	1904 06 10	5.03[a]	44.200[a]	10.842[a]	Uncertain source						
Pistoia	1904 11 17	5.15[a]	43.964[a]	10.820[a]	Uncertain source						
Po Plain	1909 01 13	5.53[a]	44.579[a]	11.688[a]	115[b]	30[b]	90[b]	4.5[b]	10.0[b]		
Murlo	1909 08 25	5.37[a]	43.150[a]	11.403[a]	Uncertain source						
Romagna	1911 02 19	5.28[a]	44.117[a]	12.075[a]	120[b]	35[b]	90[b]	4.5[b]	17.5[b]		
Romagna	1911 03 20	5.29[a]	44.133[a]	12.100[a]	120[b]	35[b]	90[b]	4.5[b]	17.5[b]		
Rimini	1911 03 26	5.00[a]	44.061[a]	12.507[a]	132[c]	30[c]	90[c]	3.0[c]	6.0[c]		
Chianti	1911 09 13	5.19[a]	43.436[a]	11.343[a]	Uncertain source						
Val Lamone	1913 07 21	4.78[a]	44.041[a]	11.762[a]	Uncertain source						
Val Taro	1913 11 25	4.84[a]	44.551[a]	10.195[a]	98[b]	35[b]	90[b]	4.5[b]	27[b]		
Garfagnana	1914 10 27	5.76[a]	43.911[a]	10.598[a]	125[b]	60[b]	−90[b]	4.5[b]	8.9[b]		
Avezzano	1915 01 13	7.00[a]	41.961[c]	13.606[c]	135[c]	60[c]	−90[c]	–	10.0[b]		
Reggio E.	1915 10 10	5.02[a]	44.732[a]	10.469[a]	110[b]	30[b]	90[b]	4.5[b]	15.9[b]		
Rimini	1916 05 17	5.95[a]	44.092[c]	12.659[b]	132[c]	30[c]	90[c]	3.0[c]	7.0[c]	−0.019/−0.003	
Rimini	**1916 08 16**	**6.14[a]**	**44.039[c]**	**12.741[c]**	**132[c]**	**30[c]**	**90[c]**	**3.0[c]**	**7.0[c]**		**0.602/1.566**
Adriatico[e]	1916 08 16	5.50[a]	44.039[e]	12.741[e]	132[e]	30[e]	90[e]	3.0[e]	7.0[e]		
Adriatico[e] (4 events)	1916 08 16	5.40[a]	44.039[e]	12.741[e]	132[e]	30[e]	90[e]	3.0[e]	7.0[e]		
Valtiberina	**1917 04 26**	**5.89[a]**	**43.479[c]**	**12.177[c]**	**315[c]**	**50[b]**	**−85[b]**	**4.5[b]**	**8.7[b]**	**0.006/0.006**	**0.048/0.058**
Romagna	**1918 11 10**	**5.88[a]**	**43.917[a]**	**11.933[a]**	**310[b]**	**65[b]**	**−95[b]**	**4.5[b]**	**10.0[b]**	**0.024/0.042**	**0.017/0.035**
Mugello	**1919 06 29**	**6.29[a]**	**43.957[a]**	**11.482[a]**	**118[b]**	**65[b]**	**−85[b]**	**5.5[b]**	**14.7[b]**	**0.006/0.012**	**0.009/0.021**
Garfagnana	1920 09 06	5.13[a]	44.250[a]	10.283[a]	244[d]	52[d]	−84[d]	4.5[b]	10.7[b]		−0.005/0.011
Garfagnana	**1920 09 07**	**6.48[a]**	**44.179[c]**	**10.315[c]**	**320[b]**	**60[b]**	**−95[b]**	**6.5[b]**	**10.2[b]**	**0.024/0.034**	**−0.009/0.031**
Lunigiana	1921 05 07	4.73[a]	44.369[c]	9.908[c]	330[b]	60[b]	−100[b]	4.5[b]	10.0[b]		0.163/0.596
Lunigiana	1921 11 29	4.63[a]	44.376[a]	9.987[a]	135[b]	60[b]	−105[b]	4.5[b]	10.0[b]		−0.103/0.724

[a] CPTI11 catalogue (Rovida et al., 2011; http://emidius.mi.ingv.it/CPTI11/).
[b] This study.
[c] DISS Working Group (2015) (version 3.2.0; http://diss.rm.ingv.it/diss/).
[d] Source parameters assumed from Stramondo et al. (2014).
[e] Group of earthquakes with Mw = 5.5 and Mw ≈ 5.4 assumed with the same hypocentral position as the Mw ≈ 6.1 main shock of August 16, 1916.

that the Coulomb stress changes produced by a normal fault rupture tend to unload at a distance across-strike normal faults falling in the negative lobes of static stress changes - regions called stress shadows (Harris, 1998) — where the Coulomb stress is reduced (see Fig. 8f).

The geometric setting of the two main fault systems is thus functional for the existence of a ~ 40–60 km-wide coupling zone in which the earthquakes produced by the axial normal faults possess the ability to transmit stresses on the external thrusts and vice versa, in a similar fashion of what inferred for the interactions between normal faulting earthquakes and eruptions of Mount Vesuvius (e.g., Nostro et al., 1998). The axial normal faults are expected to produce earthquakes with magnitude higher than the external thrusts, and are therefore believed to transmit their perturbation on the correspondent receiver faults at comparatively higher distances.

4.2. Coulomb stress changes associated with the seismic events of 1916–1920

We tested the scenarios discussed above (Section 4.1) by computing the Coulomb stress changes for the seismic events in the period

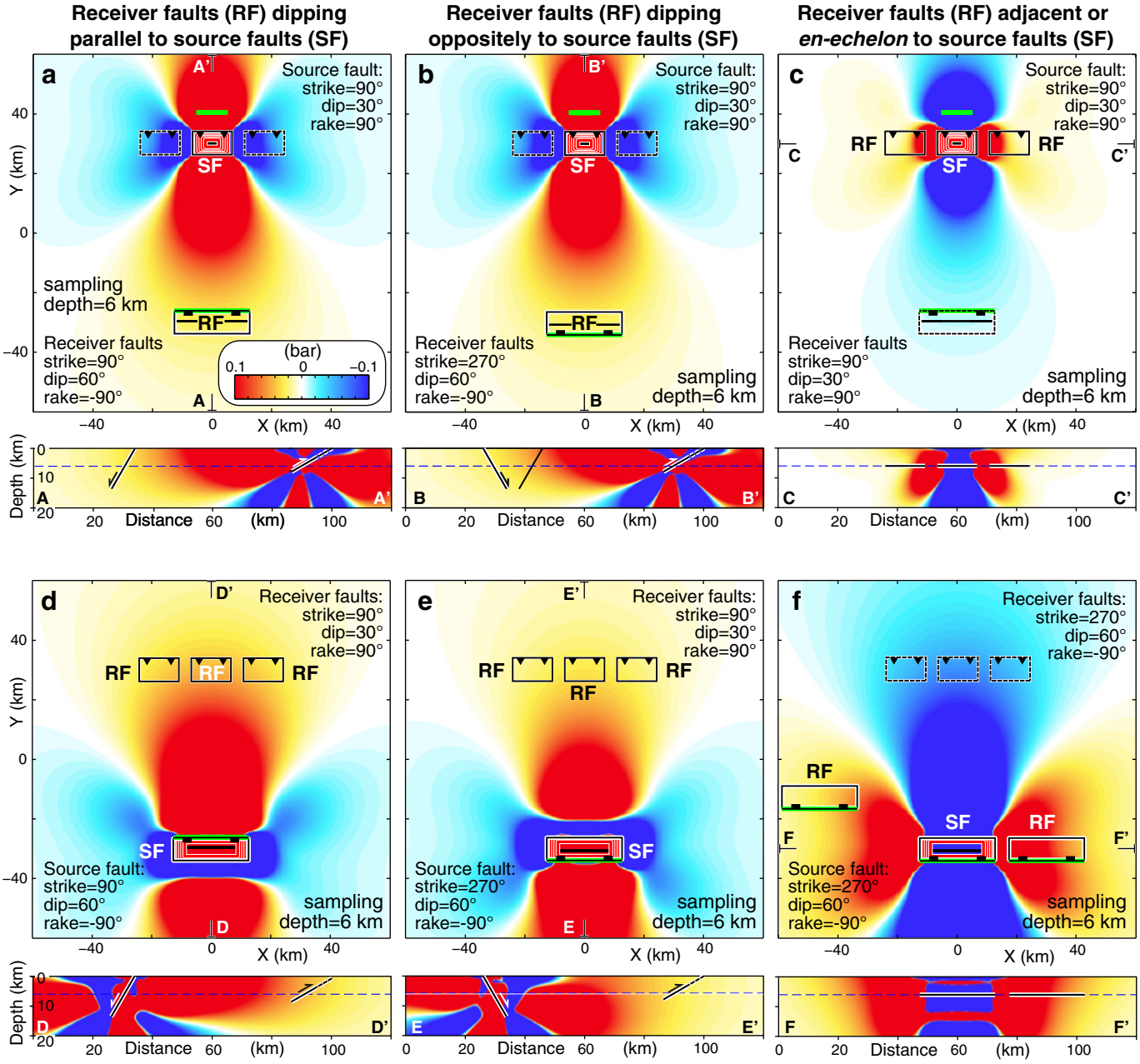

Fig. 8. Idealized cases of possible stress transfer interaction among axial normal faults and external thrusts. We have arbitrarily taken 60 km as reference distance between the source (SF) and receiver (RF) faults, which is the approximate distance between the Valtiberina normal fault and the closest external thrust of the Pede-Apennine margin. The source fault has a tapered slip, and the apparent coefficient of friction μ' is assumed to be 0.4. Coulomb stress changes caused by a Mw = 6.1 thrust earthquake on distal normal faults dipping either (a) parallel or (b) oppositely to the source fault. (c) Coulomb stress changes caused by a Mw = 6.1 thrust earthquake on adjacent, along-strike thrusts dipping parallel to the source fault. Coulomb stress changes caused by a Mw = 6.5 normal-fault earthquake on distal thrusts dipping either (d) parallel or (e) oppositely to the source fault. (f) Coulomb stress changes caused by a Mw = 6.5 normal-fault earthquake on adjacent along-strike and en-echelon normal faults with same strike, dip, and rake as the source fault.

between 1916 and 1920 (see methods in Section 2.1). The results are illustrated in chronologic order (i.e. from the oldest to youngest), and focus on the effects that a given earthquake may have produced on successive fault ruptures. The results are summarized in Table 2 (the complete dataset is reported in Table S4), where the cumulative Coulomb stress changes ΔCFF_{cum} for a given earthquake is reported as a range obtained using the following equation:

$$\Delta CFF_{cum} = \left[\sum_{i=1}^{i=N}(\Delta CFF_m - \Delta CFF_{STD})_i, \sum_{i=1}^{i=N}(\Delta CFF_m + \Delta CFF_{STD})_i\right] \quad (3)$$

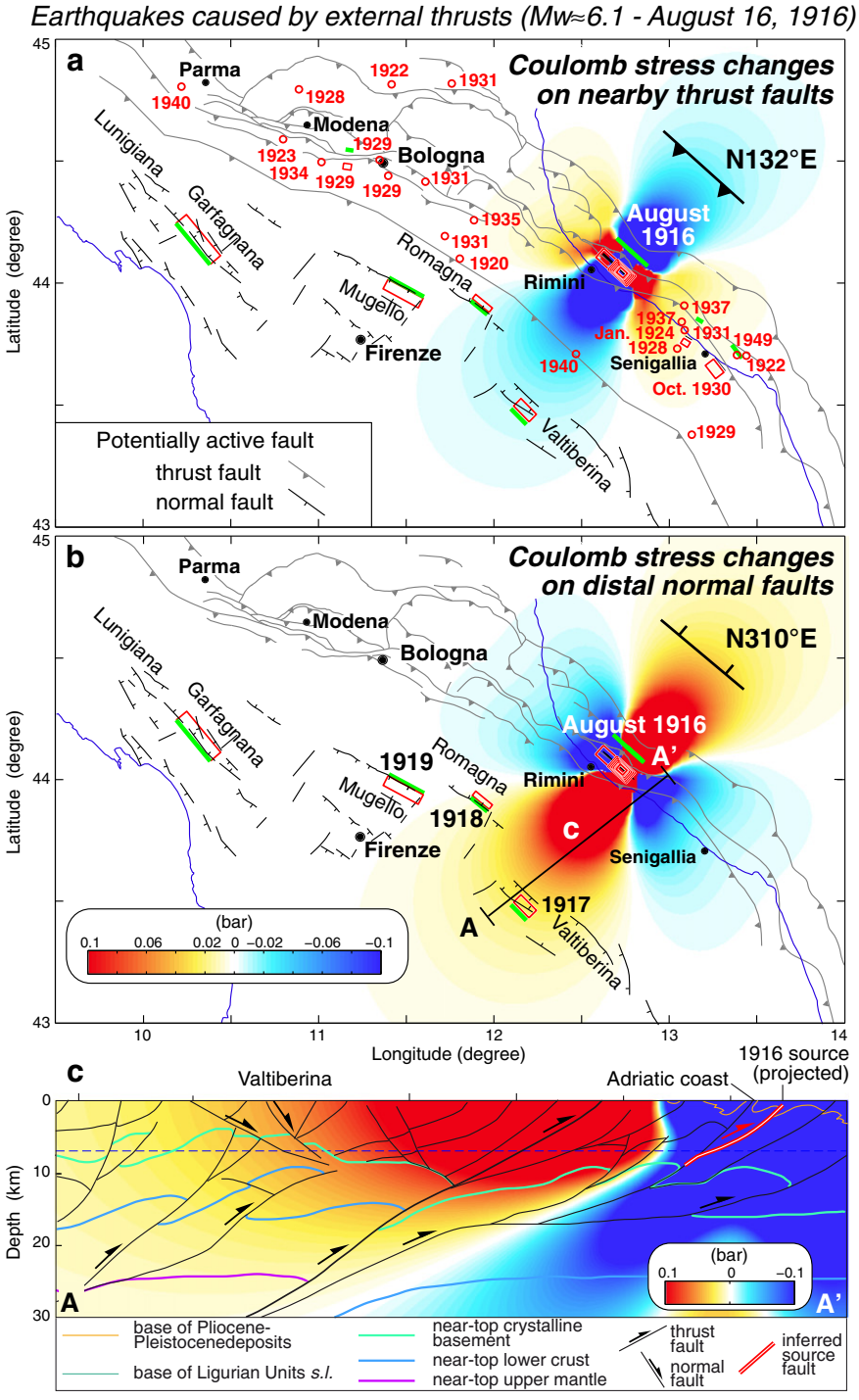

Fig. 9. Coulomb stress changes caused by rupture along thrust faults on (a) adjacent thrusts (specified fault: strike = N132°, dip = 30°, rake = 90°; depth: 5.5 km) and (b) distal (axial) normal faults (specified fault: strike = N310°, dip = 60°, rake = −90°; depth: 7 km). The causative fault is that inferred to have produced the Mw ≈ 6.1 Rimini earthquake of August 16, 1916. The open red circles indicate the epicentres of main earthquakes that hit the Pede-Apennine margin and Po Plain in the period 1920–1950 (after catalogue CPTI11; Rovida et al., 2011). Details of earthquakes and related causative faults are reported in Tables 2 and 3. (c) Coulomb stress change patterns superposed onto parts of seismic profiles CROP03 and M16 (modified from Finetti et al., 2005); the inferred causative thrust fault of the 1916 Rimini earthquake would have propagated positive stress changes up to the NE-dipping Valtiberina normal fault, which ruptured on April 26, 1917. The blue dashed line indicates the sampling depth.

where ΔCFF_m and ΔCFF_{STD} are the mean and the standard deviations of the ΔCFFs calculated for each source-receiver pair, and N is the number of earthquakes considered in the stress summation.

The results of this sensitivity analysis show that the Coulomb stress changes have a tendency to be affected by the depth variations imposed to both the source and the receiver faults (see Section 2.1). For this reason, we have not considered in the analysis those cases in which the minimum and maximum values of cumulative ΔCFF have opposite sign. Our results suggest that the 1915 Mw ≈ 7.0 Avezzano earthquake produced little effects, the magnitude of Coulomb stress changes being less than that of solid Earth tides. More specifically, the stress changes slightly discouraged faulting along the thrust segments that ruptured offshore Rimini in 1916, and loaded a little the axial normal faults that ruptured in 1917–1918 (Tables 2 and S4).

The 1916 sequence started with the Mw = 5.95 event of May 17, which loaded with more than 1 bar the nearby thrust fault. This then ruptured on August 16 producing an earthquake with Mw ≈ 6.14 (Tables 2 and S4). Both earthquakes and other minor seismic events (with Mw ≤ 5.5) raised the stress on both the Valtiberina and Romagna faults, with a magnitude of the Coulomb stress changes of the order of, or only slightly above, tidal stresses. The rupture of the Romagna fault in 1918 produced a similar increase in Coulomb stress changes on the Mugello fault that ruptured in 1919. The latter caused in turn a very small increase in stress (less than Earth tides magnitude) on both the transverse fault and the main normal fault that produced the Mw ≈ 5.1 and Mw ≈ 6.5 seismic events of September 6 and 7, 1920 (Tables 2 and S4). The Mw ≈ 6.5 seismic event, in turn, loaded with more than 0.1 bar (with maximum values of ~0.5–07 bar) the graben-bounding faults in Lunigiana, which produced two moderate earthquakes in 1921 (Fig. 7; Tables 2 and S4).

In general, the static stress changes computed for the various earthquakes are modest, and even considering the contribution of the different seismic events, which should be additive, the cumulated stress changes only seldom exceed the 'conventional' threshold of 0.1 bar (Tables 2 and S4). Some studies though have reported a correlation between stress changes caused by solid Earth tides and earthquakes (e.g., Cochran et al., 2004; Métivier et al., 2009).

Regarding the patterns of Coulomb stress changes, the results are similar to the cases idealized in Fig. 8. The stress changes diffuse both along-strike and orthogonally to the strike of the causative fault and can load or discourage faulting depending on the type and position of the receiver fault with regard to the source fault. In particular, earthquakes on external Adriatic thrust fronts are favourably oriented for transmitting positive Coulomb stress changes on both along-strike, adjacent thrust faults and distal normal faults of the axial seismogenic belt (Fig. 9a, b). The May 1916 earthquake clearly loaded the August 1916

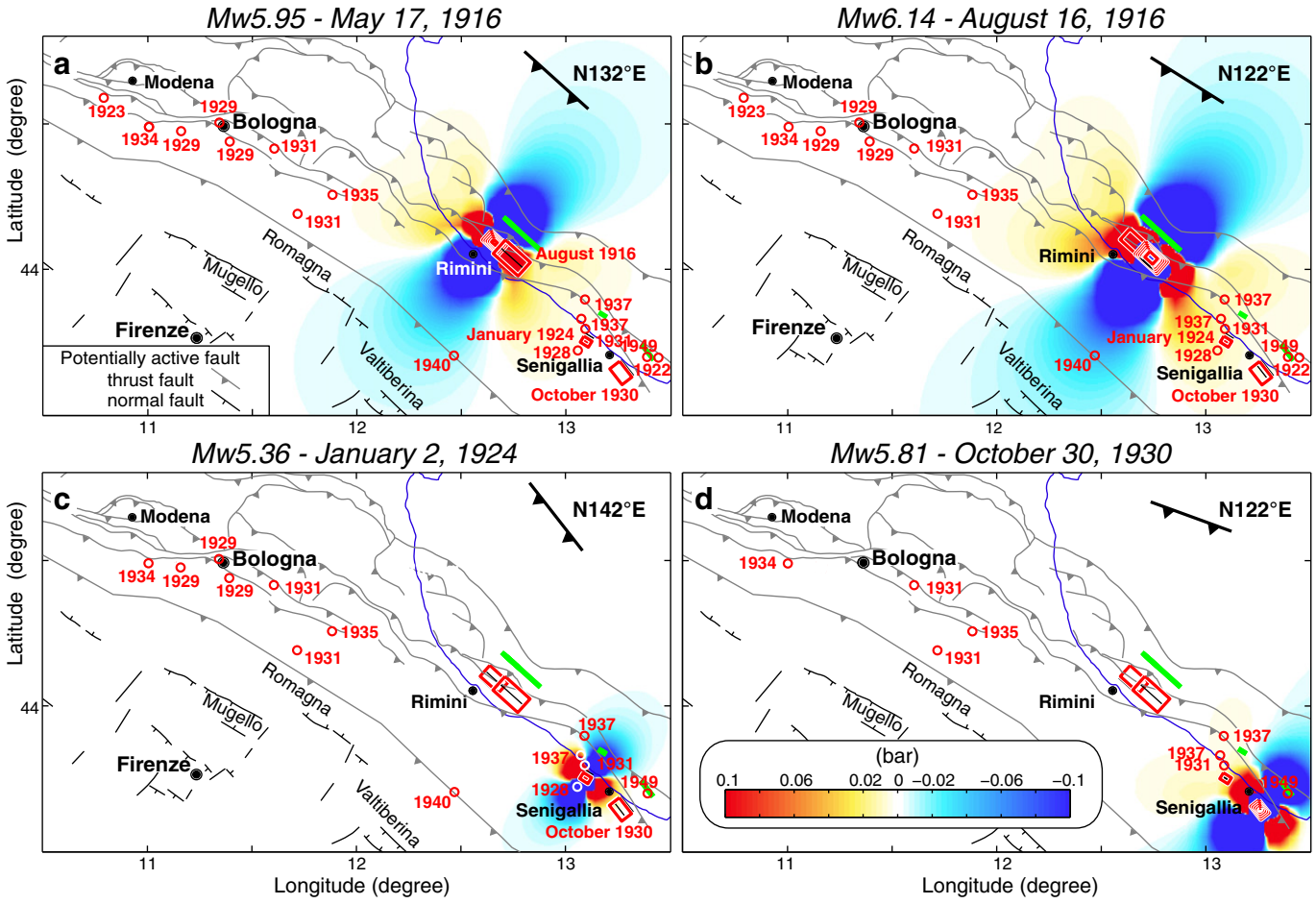

Fig. 10. Time–space progression of thrust ruptures along the external Apennine thrust front in the period 1916–1930, and the related Coulomb stress changes. (a) Mw5.95 Rimini earthquake of May 17, 1916; ΔCFF is computed on the adjacent thrust that ruptured on August 16, 1916 (specified fault strike = N132°, dip = 30°, rake = 90°; depth: 5.5 km). (b) Mw6.14 Rimini earthquake of August 16, 1916; ΔCFF is computed on the thrust that ruptured on January 1924 (specified fault: strike = N122°, dip = 30°, rake = 90°; depth: 7 km). (c) Mw5.36 Mondolfo earthquake of January 2, 1924; ΔCFF is computed on the thrust that ruptured on October 30, 1930 (specified fault: strike = N142°, dip = 30°, rake = 90°; depth: 7.5 km); (d) Mw5.81 Senigallia earthquake of October 30, 1930. The open red circles indicate the epicentres of main earthquakes that hit the Pede-Apennine margin and Po Plain in the period between 1920 and 1950 — i.e., after the end in September 1920 of the series of major extensional ruptures in the axial zone (after catalogue CPTI11; Rovida et al., 2011). Details of earthquakes and related causative faults are reported in Tables 2, 3, S4 and S5.

source, and both earthquakes loaded slightly the thrust faults that ruptured around Senigallia in 1924 and 1930 (Fig. 10; Table S5). The earthquake progression of May 1916, August 1916, January 1924 and October 1930 would suggest the possibility of along-strike stress transfer between the external thrusts, but the small values predicted for the 1924 and 1930 events introduce uncertainty to this hypothesis. As previously discussed, the Rimini seismic sequence of 1916 would have raised the stresses on some axial normal faults, particularly the Valtiberina (Fig. 9b). This process is also illustrated through the projection of the Coulomb stress change patterns onto a geological section

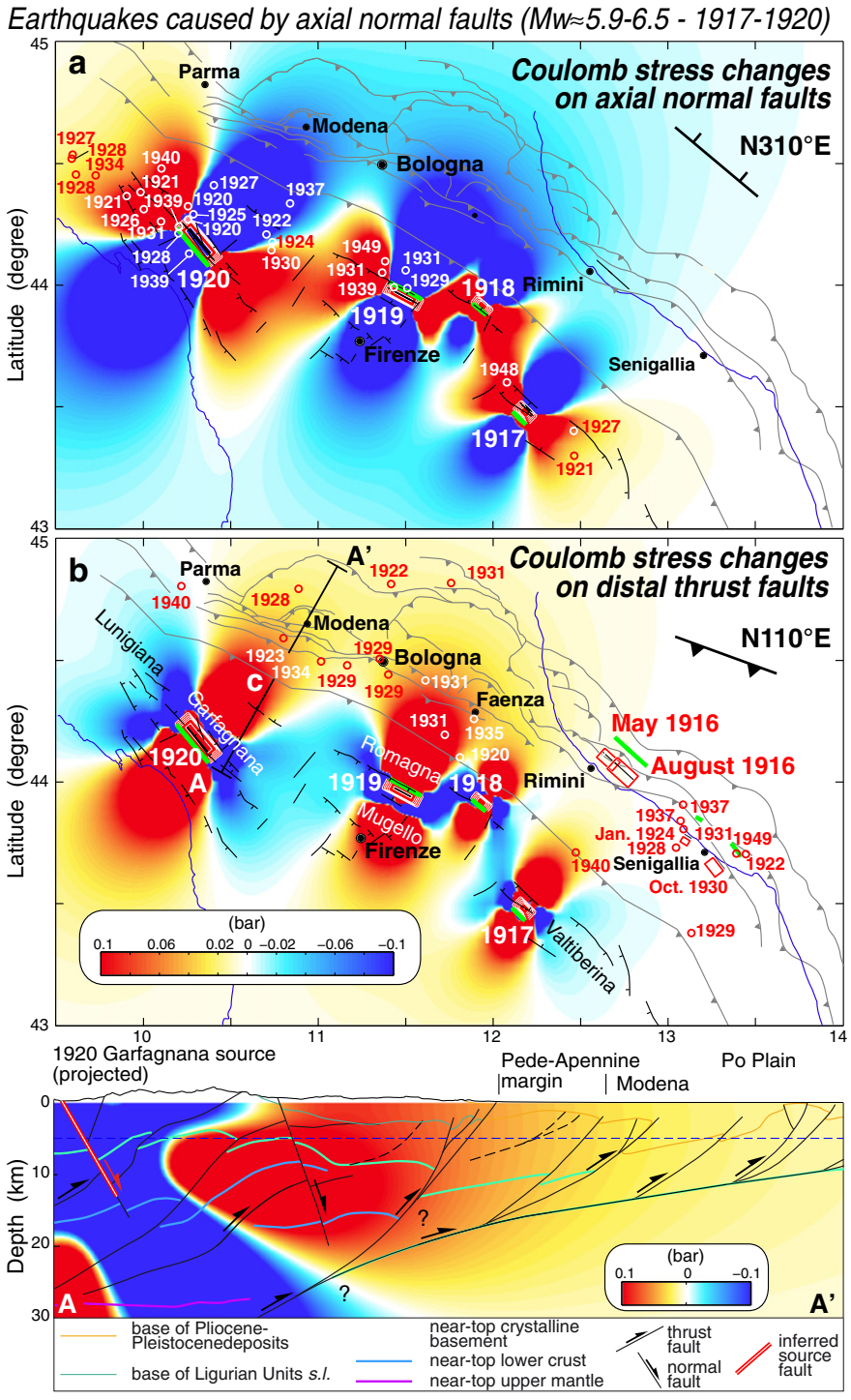

Fig. 11. Coulomb stress changes caused by rupture along axial normal faults on (a) nearby normal faults (specified fault: strike = N310°, dip = 60°, rake = −90°; depth: 7 km) and (b) distal thrust faults (specified fault: strike = N110°, dip = 30°, rake = 90°; depth: 5 km) in subsequent time windows. The causative faults are those that produced the earthquakes of Vatiberina 1917, Romagna 1918, Mugello 1919, and Garfagnana 1920. The open red circles indicate the macroseismic epicentres of earthquakes during the period between 1920 and 1950 (data from Rovida et al., 2011) falling either in the (a) internal sector dominated by normal faulting, or (b) in the external sector dominated by thrusting. The boundary between the two sectors is assumed to coincide with the most internal active thrust in the DISS catalogue (code n. ITCS027; DISS Working Group, 2015). Details of earthquakes and related causative faults are reported in Tables 2–4 and S4–S6. Symbols are as those of Figure 9. (c) Coulomb stress change patterns superposed onto a regional geological cross section (modified from Bonini, 2013). Stress changes imparted by the Mw ≈ 6.5 Garfagnana normal-fault earthquake of September 7, 1920 would have radiated on distal thrust faults of the Pede-Apennine margin and Po Plain. The blue dashed line indicates the sampling depth.

based on the interpretation of the deep seismic profiles CROP03-M16 (Finetti et al., 2001, 2005; Fig. 9c).

In the same way, earthquakes produced by the axial normal faults may bring other along–strike normal faults and also distal thrusts closer to Coulomb failure (Fig. 11a, b). The lateral transmission of stress on other normal faults is generally limited, while the effects on distal thrusts may be the most significant (see Section 5.1). The potential effects of the Mw ≈ 6.5 Garfagnana earthquake on thrusts of the Pede-Apennine margin and the Po Plain are illustrated in cross-section (Fig. 11c). The earthquakes on the axial normal faults have also the effect to produce negative Coulomb stress changes on other normal faults falling in static stress shadows orthogonal to the strike of the causative fault (see Fig. 8f). For instance, the 1919 the Mugello earthquake produced negative stress changes that would have discouraged faulting in the Firenze basin to the southwest (Boccaletti et al., 2001; Fig. 11a). These effects would be largest near the earthquake epicentre. More specifically, in an intramontane basin, negative Coulomb stress changes are conceivably highest on the normal faults that bound the margin opposite to the ruptured fault.

5. Discussion

5.1. Role of earthquakes that preceded or followed the 1916–1920 seismic cluster

A number of earthquakes predated the main seismic events of 1916–1921. We consider those in the period between 1900 and 1915. Four earthquakes with magnitude between ~5 and ~5.8 struck the Garfagnana and Lunigiana between 1902 and 1914, and two earthquakes with Mw ≈ 5.3 hit the Romagna in 1911 (Table 2). These events may have brought some normal faults closer to failure, particularly the Romagna and Garfagnana faults (Tables 2 and S4). There are however other moderate earthquakes that could have produced some stress perturbation on the faults that ruptured in 1916–1920. Unfortunately, the geometry and kinematics of many of these seismic sources are unknown or speculative (see Table 2).

After the Mw ≈ 6.5 earthquake of September 7, 1920, the seismic activity was localized in both the axial zone and the external sector. In particular, the seismicity in the external sector consisted of a series of moderate earthquakes (Mw_{MAX} ≈ 5.3) that nucleated along both the Pede-Apennine thrust and more external thrusts underneath the Po Plain (Tables 3 and S5). Seismicity along the axial zone consisted of moderate earthquakes (Mw_{MAX} ≈ 5.2) that were most likely generated by normal faults (Tables 4 and S6). The boundary between the two sectors is assumed to coincide with the most internal (i.e., southwesternmost) active thrust reported in the DISS Working Group (2015) (Fig.12a).

The distribution of the released seismic moment through time may help to decipher the possible interrelations between the 1916–1920 earthquakes and the post-1920 seismicity, part of which may have been triggered by the previous seismic events. The seismic moment M_0 is calculated using the relationship in Hanks and Kanamori (1979),

$$M_0 = 10^{(1.5Mw+16.1)} \quad [\text{dyne cm}] \tag{4}$$

where Mw is the moment magnitude. The seismic moment is calculated over the period between 1900 and 1950 and encompasses the 1916–1920 earthquake cluster, during which the released seismic moment increased dramatically (Fig. 12b). The graph also shows that the post-1920 seismic activity is essentially equivalent to the pre-1916 one. The cumulative number of earthquakes increased in 1927 up until 1932. Similarly, the cumulative seismic moment increased slightly in 1927 until 1932, after that it decays to values lower than those of pre-1916 (Fig. 12b). The delayed (post-1927) increase in the number of

Table 3
Earthquakes (period 1920–1950) that hit the external sectors of the Northern Apennines and Po Plain after the major extensional ruptures of 1917–1920 in the axial zone (macroseismic data from Rovida et al. (2011). The seismicity is calculated over the area indicated in Fig. 12a. The cumulative Coulomb stress changes (ΔCFF_{cum}) imparted by axial normal faults and/or external thrusts on the inferred receiver faults are reported. The ΔCFF_{cum} for a given earthquake is reported as a range of minimum and maximum values obtained from Eq. (3) using the mean and standard deviation associated with each source-receiver pair. The ΔCFF value loading each receiving structure by each earthquake is reported in Table S5.

Locality	Earthquake	Mw	Lat N	Long E	Inferred receiver fault					Causative faults	Cumulative ΔCFF_{cum} (bar)
					Strike (deg)	Dip (deg)	Rake (deg)	Depth (km)			
								D^1	D^2		
Modigliana	1920 06 08	4.49[a]	44.100[a]	11.800[a]	110[b]	35[b]	90[b]	4.5[b]	24.8[b]	Axial normal faults	−0.090/0.059
Ferrara	1922 05 24	4.34[a]	44.821[a]	11.408[a]	110[b]	30[b]	90[b]	4.5[b]	9.5[b]	Axial normal faults	0.013/0.013
Adriatico	1922 10 11	4.50[a]	43.700[a]	13.450[a]	122[b]	30[b]	90[b]	3.0[c]	6.5[c]	External thrusts	–
Formigine	1923 06 28	4.88[a]	44.595[a]	10.799[a]	107[b]	30[b]	90[b]	4.5[b]	15.1[b]	Axial normal faults	0.03/0.044
Mondolfo	1924 01 02	5.36[a]	43.751[c]	13.096[c]	122[c]	30[c]	90[c]	3.0[c]	7.5[c]	External thrusts	0.016/0.022
Adriatico	1928 05 30	4.88[a]	43.724[a]	13.063[a]	122[b]	30[b]	90[b]	3.0[c]	7.5[c]	External thrusts	−3.453/0.712
Carpi	1928 06 13	4.78[a]	44.797[a]	10.872[a]	80[b]	30[b]	90[b]	4.5[b]	10.0[b]	Axial normal faults	0.012/0.013
Apiro	1929 01 22	4.72[a]	43.383[a]	13.150[a]	120[c]	20[c]	90[c]	4.5[b]	10.0[b]	External thrusts	0.001/0.001
Bologna	1929 04 10	5.03[a]	44.447[a]	11.385[a]	110[b]	45[b]	90[b]	2.0[c]	8.0[c]	Axial normal faults	0.018/0.030
Bologna	1929 04 12	5.10[a]	44.500[a]	11.333[a]	98[b]	35[b]	90[b]	2.0[c]	8.0[c]	Axial normal faults	0.016/0.024
Bologna	1929 04 20	5.34[a]	44.477[c]	11.157[c]	98[c]	35[c]	90[c]	2.0[c]	8.0[c]	Axial normal faults	0.006/0.012
Senigallia	1930 10 30	5.81[a]	43.643[c]	13.260[c]	142[c]	30[c]	90[c]	3.0[c]	7.5[c]	External thrusts	0.007/0.012
Ferrara	1931 03 27	4.81[a]	44.821[a]	11.764[a]	110[b]	30[b]	90[b]	4.5[b]	10.0[b]	Axial normal faults	0.012/0.013
Faenza	1931 04 05	4.80[a]	44.194[a]	11.710[a]	105[b]	30[b]	90[b]	4.5[b]	24.8[b]	Axial normal faults	−0.061/0.174
C.S. Pietro	1931 04 11	5.10[a]	44.417[a]	11.600[a]	110[b]	30[b]	90[b]	4.5[b]	10.0[b]	Axial normal faults	0.042/0.058
Mondolfo	1931 06 25	4.51[a]	43.800[a]	13.100[a]	122[b]	30[b]	90[b]	3.0[c]	7.5[c]	External thrusts	−0.861/0.667
Vignola	1934 09 18	4.57[a]	44.495[a]	11.012[a]	98[b]	30[b]	90[b]	4.5[b]	27.9[b]	Axial normal faults	0.001/0.013
Faenza	1935 06 05	5.16[a]	44.260[a]	11.876[a]	120[b]	30[b]	90[b]	4.5[b]	7.8[b]	Axial normal faults	0.046/0.066
Adriatico	1937 02 26	4.43[a]	43.900[a]	13.100[a]	122[b]	30[b]	90[b]	3.0[c]	7.5[c]	External thrusts	−0.011/0.054
Mondolfo	1937 11 22	4.43[a]	43.833[a]	13.083[a]	122[b]	30[b]	90[b]	3.0[c]	7.5[c]	External thrusts	−0.073/0.151
Modenese	1937 12 10	5.17[a]	44.334[a]	10.834[a]	105[b]	30[b]	90[b]	4.5[b]	26.6[b]	Axial normal faults	−0.013/0.026
Noceto	1940 05 01	5.15[a]	44.800[a]	10.183[a]	125[b]	30[b]	90[b]	4.5[b]	10.0[b]	Axial normal faults	−0.011/−0.009
Urbania	1940 10 10	4.72[a]	43.700[a]	12.500[a]	130[c]	30[c]	90[c]	4.5[b]	19.1[b]	External thrusts	−0.105/0.037
										Axial normal faults	0.008/0.037
Adriatico	1949 12 06	4.50[a]	43.700[a]	13.400[a]	122[b]	30[b]	90[b]	3.0[c]	6.5[c]	External thrusts	−0.391/−0.054

[a] CPTI11 catalogue (Rovida et al., 2011; http://emidius.mi.ingv.it/CPTI11/).
[b] This study.
[c] DISS Working Group (2015) (http://diss.rm.ingv.it/diss/).

earthquakes and the rate of seismic moment release may be partly explained by static stress transfer produced by the large 1916–1920 earthquakes.

To test this hypothesis, we calculated the static stress changes produced by the various seismic sources on the inferred receiver faults, and then we considered separately the behaviour of seismic moment for the external sector (Po Plain and Pede-Apennine margin), dominated by thrusting, and the internal sector characterized by normal faulting. Static stress changes have been calculated assuming the average strike of the receiver thrust or normal fault in the epicentre area (Tables 3, 4, S5 and S6). Interestingly, many of the macroseismic epicentres of the earthquakes along the axial belt occur within fault-end Coulomb stress rise lobes (Fig.11a; Tables 4 and S6). This correlation is particularly evident northwest of the 1920 Garfagnana rupture, in Lunigiana, where the predicted positive stress changes approach and often exceed 0.1 bar (Fig. 11a and Table 4). In this case, static stress changes are large enough to suppose that they have triggered the most part of the seismicity.

This hypothesis would also agree with the trend of the seismic activity estimated for the area. This trend decays just after the large 1920 earthquake but then shows a subtle but clear increase in 1929, which is also matched by the marked increase in the number of earthquakes (Fig. 12c). However, a number of seismic events also occurred in the negative lobes of static Coulomb stress changes one or two decades after the 1919 and 1920 ruptures (Fig. 11a). The causes of these delayed earthquakes that appear in the stress shadows are not straightforward. Some of these events may be a possible effect of dynamic stresses, even though delay times between arrival of the dynamic waves and the onset of locally triggered seismicity generally vary from seconds to weeks (Hill and Prejean, 2014). The fluid flow along sub horizontal σ_2–parallel permeability that characterizes normal fault settings (Sibson, 2000) might have contributed to the triggering of a part of the events in the stress shadow near the ruptured fault.

Regarding the effects of the 1917–1920 extensional faults on the external thrusts, we have considered the part of the external sector where these ruptures are estimated to have produced some perturbation (the region extending from Parma to the south of Faenza), excluding the area where the thrust earthquakes have been dominantly loaded by larger thrust events (Fig. 12a and Tables 3 and S5). Notably, many macroseismic epicentres of thrust earthquakes fall in the Coulomb stress rise lobes of the axial normal faults (Fig. 11b, Tables 3 and S5). The hypothesis that the axial faults acted as potential triggers is corroborated by the striking increase in 1929 – a few years after the 1917–1920 series of large earthquakes – of both the released seismic moment and the number of earthquakes (Fig. 12d). Conversely, the seismic events of 1922–1937 around Rimini and Senigallia would have been loaded dominantly by the thrust earthquakes of 1916, 1924, and 1930 (Figs. 2a, 9a and 10; Table 3). The effects on the triggering caused by the Mw ≈ 5.5 Po Plain thrust earthquake of 1909 (Table 2) are negligible.

Table 4

Earthquakes that hit the axial zone of the Northern Apennines during the period from September 7, 1920 (the day of the Mw ≈ 6.5 earthquake) to 1950 (macroseismic data from Rovida et al. (2011)). The seismicity is calculated over the area indicated in Fig. 12a. The cumulative Coulomb stress changes (ΔCFF_{cum}) imparted by the 1917–1920 major extensional ruptures on the inferred receiver normal faults are reported. The ΔCFF_{cum} for a given earthquake is reported as a range of minimum and maximum values obtained from Eq. (3) using the mean and standard deviation associated with each source-receiver pair. The ΔCFF value loading each receiving structure by each earthquake is reported in Table S6. Owing to the uncertain hypocentral localization, static stress changes are not calculated when the seismic events fall along the boundary between positive and negative lobes of Coulomb stress changes (see Fig.11a).

Locality	Earthquake	Mw	Lat N	Long E	Inferred receiver fault					Cumulative ΔCFF_{cum} (bar)
					Strike (deg)	Dip (deg)	Rake (deg)	Depth (km)		
								D^1	D^2	
Garfagnana	1920 09 07	4.96[a]	44.250[a]	10.283[a]	135[b]	60[b]	−90[b]	4.5[b]	10.7[b]	–[c]
Garfagnana	1920 09 07	4.68[a]	44.250[a]	10.283[a]	135[b]	60[b]	−90[b]	4.5[b]	10.7[b]	–[c]
Garfagnana	1920 09 07	4.73[a]	44.317[a]	10.283[a]	320[b]	60[b]	−90[b]	4.5[b]	13.7[b]	0.329/1.145
Garfagnana	1920 12 27	4.76[a]	44.250[a]	10.283[a]	135[b]	60[b]	−90[b]	4.5[b]	10.7[b]	–[c]
Castiglione	1921 04 05	4.72[a]	43.300[a]	12.500[a]	130[d]	20[d]	−90[d]	4.5[b]	9.0[b]	0.011/0.021
Lunigiana	1921 05 07	4.73[a]	44.369[d]	9.908[d]	330[b]	60[b]	−100[b]	4.5[b]	10.0[b]	0.099/0.144
Lunigiana	1921 11 29	4.63[a]	44.376[a]	9.987[a]	135[b]	60[b]	−105[b]	4.5[b]	10.0[b]	0.111/0.174
Pievepelago	1922 08 02	4.68[a]	44.200[a]	10.700[a]	305[b]	60[b]	−90[b]	4.5[b]	16.2[b]	−0.133/0.059
Fanano	1924 06 12	4.86[a]	44.167[a]	10.733[a]	305[b]	60[b]	−90[b]	4.5[b]	14.8[b]	–[c]
Frassinoro	1925 03 15	4.52[a]	44.282[a]	10.286[a]	125[b]	60[b]	−90[b]	4.5[b]	10.7[b]	−1.026/4.329
Bagnone	1926 11 18	4.51[a]	44.300[a]	10.000[a]	135[b]	60[b]	−105[b]	4.5[b]	10.0[b]	0.169/0.335
Bedonia	1927 10 28	4.88[a]	44.520[a]	9.590[a]	300[b]	60[b]	−90[b]	4.5[b]	10.9[b]	0.018/0.014
Cervarezza	1927 11 20	4.68[a]	44.400[a]	10.400[a]	305[b]	60[b]	−90[b]	4.5[b]	23.9[b]	−0.281/0.13
Mt. Leto	1927 11 30	4.72[a]	43.400[a]	12.500[a]	130[b]	60[b]	−90[b]	4.5[b]	8.6[b]	0.034/0.047
Varese L.	1928 02 21	4.39[a]	44.440[a]	9.611[a]	300[b]	60[b]	−90[b]	4.5[b]	11.3[b]	0.022/0.026
Val di Taro	1928 07 20	4.46[a]	44.508[a]	9.587[a]	300[b]	60[b]	−90[b]	4.5[b]	10.9[b]	0.015/0.018
Fivizzano	1928 08 03	4.51[a]	44.200[a]	10.200[a]	320[b]	60[b]	−95[b]	4.5[b]	10.3[b]	–[c]
Mugello	1929 07 18	5.02[a]	43.988[a]	11.507[a]	118[b]	65[b]	−85[b]	4.5[b]	9.5[b]	−6.165/4.448
Fiumalbo	1930 05 24	4.81[a]	44.136[a]	10.724[a]	320[b]	60[b]	−90[b]	4.5[b]	14.8[b]	−0.049/0.1049
Fivizzano	1931 01 25	4.68[a]	44.250[a]	10.100[a]	135[b]	60[b]	−105[b]	4.5[b]	10.1[b]	0.082/0.488
Mugello	1931 09 05	4.80[a]	44.057[a]	11.367[a]	293[b]	75[b]	−90[b]	4.5[b]	12.5[b]	0.023/0.222
Mugello	1931 12 15	4.85[a]	44.070[a]	11.494[a]	300[b]	60[b]	−90[b]	4.5[b]	11.0[b]	−3.313/0.286
Val di Taro	1934 06 13	4.99[a]	44.438[a]	9.725[a]	300[b]	60[b]	−90[b]	4.5[b]	11.1[b]	0.028/0.034
Pavullo	1937 12 10	5.17[a]	44.334[a]	10.834[a]	300[b]	60[b]	−90[b]	4.5[b]	26.0[b]	−0.101/−0.037
Mugello	1939 02 11	5.01[a]	44.002[a]	11.431[a]	118[b]	65[b]	−85[b]	4.5[b]	11.0[b]	−16.69/4.219
Garfagnana	1939 10 15	5.08[a]	44.119[a]	10.255[a]	320[b]	60[b]	−90[b]	4.5[b]	10.2[b]	−9.797/−0.257
Versilia	1939 10 31	4.99[a]	44.233[a]	10.200[a]	320[b]	60[b]	−90[b]	4.5[b]	10.3[b]	–[c]
Corniglio	1940 01 24	5.03[a]	44.467[a]	10.100[a]	310[b]	60[b]	−90[b]	4.5[b]	23.8[b]	0.078/0.112
Valtiberina	1948 06 13	5.05[a]	43.598[a]	12.127[a]	130[b]	50[b]	−90[b]	4.5[b]	9.6[b]	0.155/0.246
Firenzuola	1949 03 09	4.76[a]	44.100[a]	11.383[a]	310[b]	60[b]	−90[b]	4.5[b]	18.7[b]	0.129/0.355

[a] CPTI11 catalogue (Rovida et al., 2011; http://emidius.mi.ingv.it/CPTI11/).
[b] This study.
[c] ΔCFF not calculated because the seismic event lies along the boundary between positive and negative lobes of Coulomb stress changes.
[d] DISS Working Group (2015) (http://diss.rm.ingv.it/diss/).

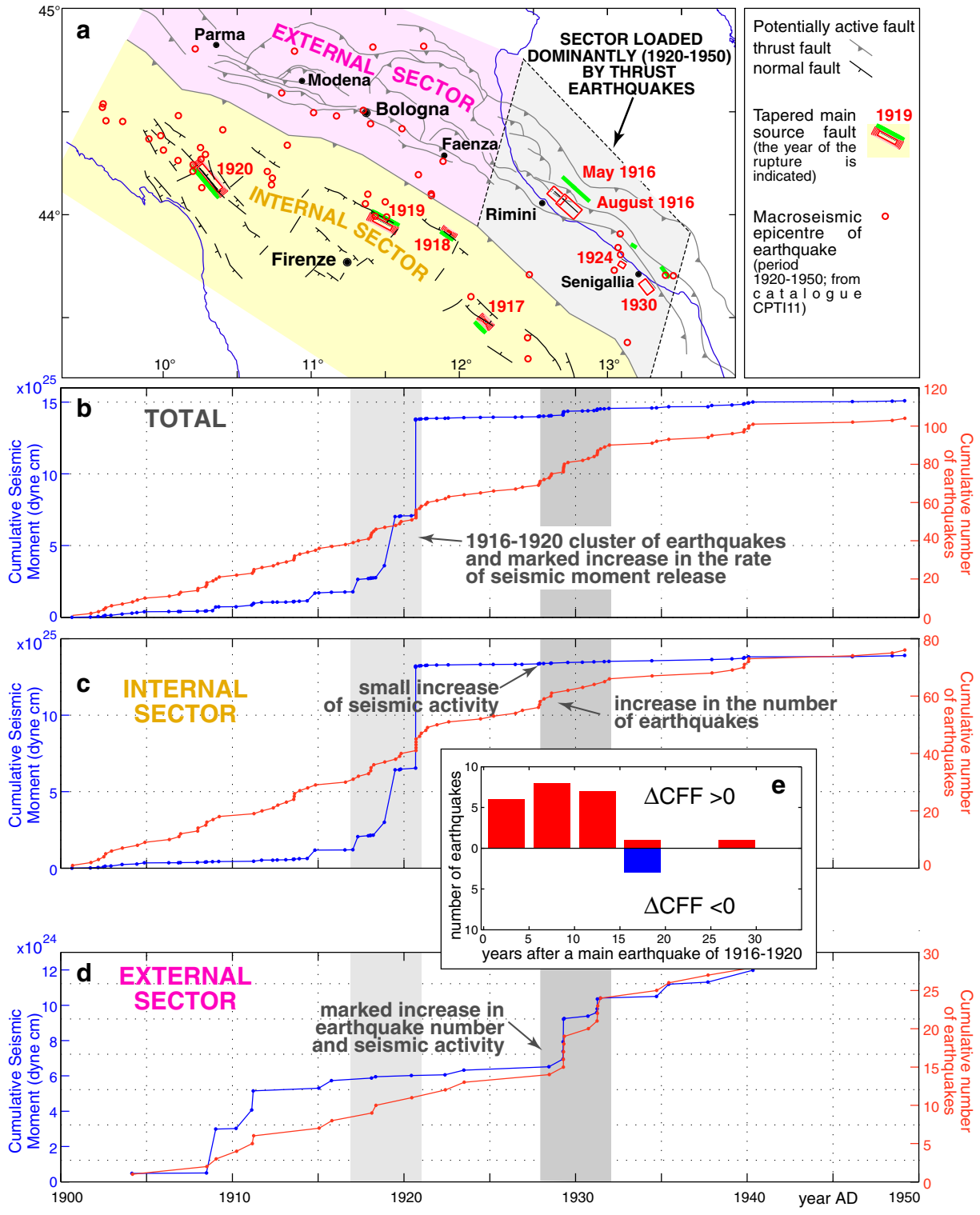

Fig. 12. (a) Distribution of seismicity in the period between 1920 and 1950 (from catalogue CPTI11; Rovida et al., 2011). (b) Cumulative number of earthquakes and seismic moment (Hanks and Kanamori, 1979) calculated over the area shown in panel (a); the magnitude of the single earthquakes is shown in Fig. 1b. Note the sharp increase in the rate of seismic moment release during the period between 1916 and 1920. (c) Cumulative number of earthquakes and seismic moment calculated over the internal sector of the Northern Apennines (yellowish area), characterized by normal faulting. (d) Cumulative number of earthquakes and seismic moment calculated over a part of the external sector of the Northern Apennines, where the 1917–1920 extensional axial ruptures are inferred to have raised the stress on the active thrust faults (pink area). The part of the external sector where the thrust earthquakes have been dominantly triggered by larger thrust events (grey area) is not considered in this analysis. The boundary between the internal and external sectors is assumed to coincide with the most internal (i.e., south-westernmost) active thrust in the DISS catalogue (code n. ITCS027; DISS Working Group, 2015). (e) Time distribution of earthquakes (bin size is 5 years) that occurred in areas (both pink and yellow sectors in panel a) with positive or negative ΔCFF created by the main extensional ruptures of 1917–1920. The earthquakes with positive ΔCFF show the main frequency peaks during 15 years after the major triggering seismic events, and then the number of events decreases with time. This analysis has concerned only those cases (reported in Tables 3 and 4) for which the minimum and maximum values of cumulative ΔCFF have the same sign.

Fig. 12e shows a simple time distribution of earthquakes falling in areas with positive or negative ΔCFF created by the main extensional seismic events of 1917–1920 (the area considered for this analysis includes both the pink and yellow sectors in Fig.12a). In this analysis we have considered only the events (reported in Tables 3 and 4) that show the minimum and maximum values of cumulative stress change range with the same sign. The majority of the earthquakes occur in areas with positive ΔCFF. In particular, the earthquakes with ΔCFF > 0 show the main frequency peaks over the 15 years after the main triggering seismic events, and afterwards the number of earthquakes decays with time. The number of earthquakes with ΔCFF < 0 is subordinate and, these ones occur in a single cluster 15 years after the supposed triggering events (Fig. 12e).

5.2. Considerations on the role of Coulomb stress changes in the 1916–1920 earthquake cluster

All the faults that ruptured during 1916–1921 were brought closer to Coulomb failure by the coseismic stresses produced by previous earthquakes. The possibility to relate this series of earthquakes to a domino-like behaviour is appealing but equivocal in that, apart from a few exceptions, the magnitude of the Coulomb stress changes is modest. The cumulated Coulomb stress changes, in fact, rarely reach the threshold of 0.1 bar that has been suggested in a number of case studies of earthquake triggered by static stresses (e.g., Stein, 1999). In the majority of cases, the static stresses are only somewhat higher than tidal stresses, while some earthquakes transmitted little or no calculated stress changes. For instance, the 1918 Romagna earthquake loaded the Mugello faults very weakly, and similarly the 1919 Mugello earthquake loaded the Garfagnana faults with very low stress changes, making it difficult to infer a causative relationship for these seismic events (Tables 2 and S4).

Notwithstanding the modest magnitude, Coulomb stress changes have loaded all the ruptures occurred between 1916 and 1921, therefore we cannot exclude that these stresses have played some role in the triggering of at least part of the seismic events. In addition, if the Coulomb stress changes produced by any earthquake are cumulative, even small stress increases may 'advance the clock' of the next seismic event. It is however unknown whether the considered faults exhibit such a sensitivity. Nevertheless, the increase in seismic activity observed in both the internal and the external sectors a few years after the 1916–1920 ruptures, and the location of many earthquake epicentres in the lobes of Coulomb stress rise (see Section 5.1), seem to support the action of permanent static stress changes. The dynamic stresses due to the passage of seismic waves should not produce permanent changes in stress, unless they modify the mechanical properties of the crust, or involve the transport and excitation of the crustal fluids.

We unfortunately lack information on the stress conditions of the normal faults and thrusts prior to failure. The 1916 earthquakes along the compressive external Adriatic belt raised the stress on the Valtiberina fault more than at any other normal fault. This fact may be compatible with the activation of this fault as the first of the series of strong earthquakes that continued with the north-westward propagation of the faulting along the belt of intramontane basins (Table 2). It is also worth noting that some earthquakes raised the stress on the Romagna and Garfagnana normal faults prior to 1916 (see Section 5.1; Tables 2 and S4), and thus may have prepared the faults to be triggered off. Last but not least, other mechanisms could have interacted with the static stress changes and contributed to the triggering, particularly the significant clock advance potentially produced by dynamic stress changes (e.g., Hill and Prejean, 2014), and the strain and strain rate perturbation caused by viscoelastic relaxation of coseismic shear stresses (Viti et al., 2012).

The results of our numerical modelling suggest that, regardless of the 1916–1920 seismic events, earthquakes along the thrust faults – if of suitable magnitude – may have the ability to transfer stress on normal faults settled in the interior of the chain and vice versa. As a corollary, earthquakes produced along the compressive thrust fronts may initiate earthquake sequences in more internal sectors of the belt situated roughly orthogonal to the source fault strike, as could have happened for the loading of the Valtiberina fault by the Rimini earthquakes of 1916. The correlation between the stress changes produced by the 1917–1920 extensional ruptures and the earthquakes on the external thrusts finalizes the hypothesis of a two-way interaction between external thrusts and axial faults. This study is certainly not conclusive, and for many aspects it represents only a working hypothesis. The acquisition of more detailed data on magnitude, location and geometry of the source faults could contribute to achieve a clearer picture of the causes that led to the lethal chain of seismic events of 1916–1920.

6. Conclusions

Geological and structural data collected on the active faults in the axial and the frontal sectors of the Northern Apennines allowed us to better characterize their geometry and kinematics. The Coulomb stress changes produced by the large earthquakes that hit the Northern Apennines in the period between 1916 and 1920 have been evaluated on the basis of the source faults reported in the literature and surveyed and/or determined in this study. The results suggest the existence of a ~40–60 km-wide coupling zone in which the earthquakes of magnitude ~6 or higher produced by axial normal faults can load thrust segments of the external thrust fronts and vice versa. The static stress change patterns produced by earthquakes along the Adriatic thrust fronts are favourable for transmitting positive Coulomb stress changes on both along-strike, adjacent thrust faults and distal normal faults of the seismogenic axial belt. Earthquakes produced by the axial normal faults may bring other along–strike normal faults as well as distal thrusts closer to Coulomb failure. The faults that generated the main seismic events between 1916 and 1921 were brought closer to failure by previous earthquakes, but the magnitude of the Coulomb stress changes is generally modest or even negligible, and only seldom exceeds the conventional threshold of 0.1 bar. The role of Coulomb stress changes in the development of the 1916–1920 earthquake cluster is at the moment equivocal, even though stress changes would have played a role in the triggering of specific earthquakes of this series, particularly the events of Rimini (August) 1916, Lunigiana 1921, and perhaps Valtiberina 1917. In addition, preparatory seismic events loaded some of the faults that ruptured between 1917 and 1920 (particularly Romagna and Garfagnana), thus raising the possibility that the peculiar time–space progression of the main seismic shocks between 1916 and 1921 was fortuitous. We are also aware of the problems resulting from the uncertainties about the parameters of the historical sources, which obviously affect the calculation of the Coulomb stress changes. Therefore, the exercise carried out in this study should be viewed only as an attempt to elaborate a model based on the status of the present knowledge. More detailed information on the parameters of the seismic sources (i.e., location, geometry, kinematics and earthquake magnitude) may refine/improve the results and provide further insights for deciphering the dynamics and the conditions that led to this harmful succession of seismic events.

Acknowledgements

We thank the anonymous reviewers for the constructive comments that helped to clarify several points. The revision of the English text by Mariolina Mousaw is gratefully acknowledged. Part of this research has been funded within the contract between the Consiglio Nazionale delle Ricerche, Istituto di Geoscienze e Georisorse, and Regione Emilia-Romagna, Servizio Geologico, Sismico e dei Suoli (Contract CUP: E59D14000510002).

Appendix A. Supplementary data

Supplementary data to this article can be found online at http://dx.doi.org/10.1016/j.tecto.2016.04.045.

References

Amato, A., Antonioli, A., Chiaraluce, L., De Gori, P., Di Stefano, R., Doumaz, F., Faenza, L., Lauciani, V., Marchetti, A., Mele, F., Michelini, A., Pirro, M., Scognamiglio, L., Selvaggi, G., Valoroso, L., Vinci, S., Anselmi, M., De Rubeis, V., Piccinini, D., Sbarra, P., Tinti, E., Tosi, P., Fiaschi, A., 2008. Rapporto Tecnico-Scientifico sulla Sequenza Sismica del Mugello del 1 Marzo 2008. Istituto Nazionale di Geofisica e Vulcanologia (30 pp).

Aki, K., Richards, P.G., 1980. Quantitative Seismology, Theory and Methods. W.H. Freeman & Co., New York (932 pp).

Argnani, A., Barbacini, G., Bernini, M., Camurri, F., Ghielmi, M., Papani, G., Rizzini, F., Rogledi, S., Torelli, L., 2003. Gravity tectonics driven by quaternary uplift in the Northern Apennines: insights from the La Spezia-Reggio Emilia geo-transect. Quat. Int. 101–102, 13–26.

Artoni, A., Bernini, M., Papani, G., Vescovi, P., Zanzucchi, G., 1992. Sezione geologica schematica Bonassola (SP)-Felino (PR). Studi Geol. Camerti 1992 (2), 61–63.

Barberi, F., Scandone, P. (Eds.), 1983. Structural Model of Italy, Scale 1:500,000, Progetto Finalizzato Geodinamica. Consiglio Nazionale delle Ricerche, Rome.

Barchi, M.R., Ciaccio, M.G., 2009. Seismic images of an extensional basin, generated at the hangingwall of a low-angle normal fault: the case of the Sansepolcro basin (Central Italy). Tectonophysics 479, 285–293.

Bartolini, C., Bernini, M., Carloni, G.C., Costantini, A., Federici, P.R., Gasperi, G., Lazzarotto, A., Marchetti, G., Mazzanti, R., Papani, G., Pranzini, G., Rau, A., Sandrelli, F., Vercesi, P.L., Castaldini, D., Francavilla, F., 1982. Carta neotettonica dell'Appennino settentrionale. Bollettino della Società Geologica Italiana 101, 523–549.

Basili, R., Valensise, G., Vannoli, P., Burrato, P., Fracassi, U., Mariano, S., Tiberti, M.M., Boschi, E., 2008. The Database of Individual Seismogenic Sources (DISS), version 3: summarizing 20 years of research on Italy's earthquake geology. Tectonophysics 453, 20–43.

Benedetti, L.C., Tapponnier, P., Gaudemer, Y., Manighetti, I., Van derWoerd, J., 2003. Geomorphic evidence for an emergent active thrust along the edge of the Po Plain: the Broni–Stradella fault. J. Geophys. Res. 108, 2238. http://dx.doi.org/10.1029/2001JB001546.

Benini, A., Farabegoli, E., 1991. Tettonica trasversale nell'Appennino forlivese. La Linea del Bidente. Memorie Descrittive della Carta Geologica d'Italia 46, 245–255.

Benvenuti, M., Papini, M., 1997. Depositi continentali plio-pleistocenici nell'area di Monte Giovi. Relazione tra l'evoluzione idrografica e la neotettonica della Valdisieve (Firenze). Il Quaternario 10, 105–120.

Bernini, M., Lasagna, S., 1988. Rilevamento geologico e analisi strutturale del Bacino dell'alta Val Magra Tra M. Orsaro e Pontremoli (Appennino Settentrionale). Atti Società Toscana di Scienze Naturali, Memorie Serie a Vol. 95, pp. 139–183.

Bernini, M., Papani, G., 2002. La distensione della fossa tettonica della Lunigiana nord-occidentale (con carta geologica alla scala 1:50,000) Bollettino della Società Geologica Italiana. Vol. 121 pp. 313–341.

Boccaletti, M., Corti, G., Martelli, L., 2011. Recent and active tectonics of the external zone of the Northern Apennines (Italy). Int. J. Earth Sci. 100, 1331–1348.

Boccaletti, M., Bonini, M., Corti, G., Gasperini, P., Martelli, L., Piccardi, L., Tanini, C., Vannucci, G., 2004. Seismotectonic Map of the Emilia–Romagna Region, Scale 1: 250,000, with Explanatory Notes. S.EL.CA, Società Elaborazioni Cartografiche, Firenze, Italy.

Boccaletti, M., Corti, G., Gasperini, P., Piccardi, L., Vannucci, G., Clemente, S., 2001. Active tectonics and seismic zonation and of the urban area of Florence (Italy). Pure Appl. Geophys. 158, 2313–2332.

Boncio, P., Brozzetti, F., Lavecchia, G., 2000. Architecture and seismotectonics of a regional low-angle normal fault zone in central Italy. Tectonics 19, 1038–1055.

Bonini, M., 2009. Structural controls on a carbon dioxide-driven mud volcano field in the Northern Apennines (Pieve Santo Stefano, Italy): relations with pre-existing steep discontinuities and seismicity. J. Struct. Geol. 31, 44–54.

Bonini, M., 2013. Fluid seepage variability across the external Northern Apennines (Italy): structural controls with seismotectonic and geodynamic implications. Tectonophysics 590, 151–174.

Brozzetti, F., Boncio, P., Lavecchia, G., Pace, B., 2009. Present activity and seismogenic potential of a low-angle normal fault system (Città di Castello, Italy): constraints from surface geology, seismic reflection data and seismicity. Tectonophysics 463, 31–46.

Burrato, P., Ciucci, F., Valensise, G., 2003. An inventory of river anomalies in the Po Plain, northern Italy: evidence for active blind thrust faulting. Ann. Geophys. 46, 865–882.

Calistri, M., 1974. Studi di Geomorfologia e Neotettonica. II - Il Pliocene fluvio-lacustre della conca di Barga. Memorie della Società Geologica Italiana Vol. 13, pp. 1–21.

Capacci, C., 1920. Osservazioni geotettoniche sul terremoto mugellano del 29 Giugno 1919. Atti della Reale Accademia dei Georgofili, Firenze, pp. 182–194.

Cattuto, C., Cencetti, C., Fisauli, M., Gregori, L., 1995. I Bacini pleistocenici di Anghiari e Sansepolcro nell'alta valle del Tevere. Il Quaternario 8, 119–128.

Chiarabba, C., Jovane, L., DiStefano, R., 2005. A new view of Italian seismicity using 20 years of instrumental recordings. Tectonophysics 395, 251–268.

Ciaccio, M.G., Chiarabba, C., 2002. Tomographic models and seismotectonics of the Reggio Emilia region, Italy. Tectonophysics 344, 261–276.

Ciaccio, M.G., Pondrelli, S., Frepoli, A., 2006. Earthquake fault-plane solutions and patterns of seismicity within the Umbria Region, Italy. Ann. Geophys. 49, 987–1002.

Cocco, M., Rice, J.R., 2002. Pore pressure and poroelasticity effects in Coulomb stress analysis of earthquake interactions. J. Geophys. Res. 107, 2030. http://dx.doi.org/10.1029/2000JB000138.

Cochran, E.S., Vidale, J.E., Tanaka, S., 2004. Earth tides can trigger shallow thrust fault earthquakes. Science 306, 1164–1166.

Corti, G., Lucia, S., Bonini, M., Sani, F., Mazzarini, F., 2006. Interaction between normal faults and pre-existing thrust systems in analogue models. In: Buiter, S.J.H., Schreurs, G. (Eds.), Analogue and Numerical Modelling of Crustal-Scale Processes Vol. 253. Geological Society of London, Special Publications, pp. 65–78.

Dallan, L., Nardi, R., 1974. Schema stratigrafico e strutturale dell'Appennino settentrionale. Memorie dell'Accademia Lunigianense di Scienze 'G. Cappellini'. La Spezia XLII-1972, 1–212.

Delle Donne, D., 2005. Tettonica attiva dell'Appennino Settentrionale nel settore compreso tra l'Appennino Pistoiese e l'alta Val Tiberina. Università degli Studi di Firenze (Unpublished PhD Thesis, 144 pp).

Delle Donne, D., Piccardi, L., Odum, J.K., Stephenson, W.J., Williams, R.A., 2007. High resolution shallow reflection seismic image and surface evidence of the Upper Tiber Basin active faults (Northern Apennines, Italy). Bollettino della Società Geologica Italiana 126, 323–331.

Di Naccio, D., Boncio, P., Brozzetti, F., Pazzaglia, F.J., Lavecchia, G., 2013. Morphotectonic analysis of the Lunigiana and Garfagnana grabens (northern Apennines, Italy): implications for active normal faulting. Geomorphology 201, 293–311.

DISS Working Group, 2015. Database of Individual Seismogenic Sources (DISS), Version 3.2.0: a compilation of potential sources for earthquakes larger than M 5.5 in Italy and surrounding areas. http://diss.rm.ingv.it/diss/, © INGV 2015 - Istituto Nazionale di Geofisica e Vulcanologia; DOI:10.6092/INGV.IT-DISS3.2.0.

Doglioni, C., Barba, S., Carminati, E., Riguzzi, F., 2014. Fault on–off versus coseismic fluids reaction. Geosci. Front. 5, 767–780. http://dx.doi.org/10.1016/j.gsf.2013.08.004.

Eva, C., Giglia, G., Graziano, F., Merlanti, F., 1978. Seismicity and its relation with surface structures in the north-western Apennines. Boll. Geofis. Teor. Appl. 79, 263–277.

Eva, E., Solarino, S., Boncio, P., 2014. HypoDD relocated seismicity in northern Apennines (Italy) preceding the 2013 seismic unrest: seismotectonic implications for the Lunigiana-Garfagnana area. Boll. Geofis. Teor. Appl. 55, 739–754.

Fantoni, R., Franciosi, R., 2010. Tectono-sedimentary setting of the Po Plain and Adriatic foreland. Rend. Fis. Acc. Lincei 21 (1), S197–S209.

Finetti, I., Boccaletti, M., Bonini, M., Del Ben, A., Geletti, R., Pipan, M., Sani, F., 2001. Crustal section based on CROP seismic data across the North Tyrrhenian–Northern Apennines–Adriatic Sea. Tectonophysics 343, 135–163.

Finetti, I.R., Boccaletti, M., Bonini, M., Del Ben, A., Pipan, M., Prizzon, A., Sani, F., 2005. Chapter 8 — lithospheric tectono-stratigraphic setting of the Ligurian Sea — Northern Apennines — Adriatic foreland from integrated CROP seismic data. In: I., F. (Ed.), CROP Project — Deep Seismic Exploration of the Central Mediterranean and Italy. Atlases in Geoscience 1. Elsevier B.V., pp. 119–158 (ISBN: 0-444-50693-4).

Galli, P., Meloni, F., 1993. Nuovo catalogo nazionale dei processi di liquefazione avvenuti in occasione dei terremoti storici in Italia. Il Quaternario 6, 271–292.

Gasperini, P., Bernardini, F., Valensise, G., Boschi, E., 1999. Defining seismogenic sources from historical earthquake felt reports. Bull. Seismol. Soc. Am. 89, 94–110.

Gasperini, P., Vannucci, G., Tripone, D., Boschi, E., 2010. The location and sizing of historical earthquakes using the attenuation of macroseismic intensity with distance. Bull. Seismol. Soc. Am. 100 (5A), 2035–2066.

Gunderson, K.L., Anastasio, D.A., Pazzaglia, F.J., Picotti, V., 2013. Fault slip rate variability on 104–105 yr timescales for the Salsomaggiore blind thrust fault, Northern Apennines, Italy. Tectonophysics 608, 356–365.

Hanks, C., Kanamori, H., 1979. A moment magnitude scale. J. Geophys. Res. 84, 2348–2350.

Harris, R.A., 1998. Introduction to special section: stress triggers, stress shadows and implications for seismic hazard. J. Geophys. Res. 103, 24,347–24,358.

Hill, D.P., Prejean, S.G., 2014. Dynamic triggering. Treatise on geophysics. Earthquake Seismology. Vol. 4, pp. 257–291 Chapter 9.

Kilb, D., Gomberg, J., Bodin, P., 2002. Aftershock triggering by complete coulomb stress changes. J. Geophys. Res. 107, 2060. http://dx.doi.org/10.1029/2001JB000202.

King, G.C.P., 2014. Fault interaction, earthquake stress changes, and the evolution of seismicity. Treatise on geophysics. Earthquake Seismology. Vol. 4, pp. 225–255 Chapter 8.

King, G.C.P., Stein, R.S., Lin, J., 1994. Static stress changes and the triggering of earthquakes. Bull. Seismol. Soc. Am. 84, 935–953.

Landuzzi, A., 1991. Structural setting and landforms in the Marnoso-Arenacea of the Alta Romagna Apennines (Italy): an approach to neo-tectonics. Bollettino della Società Geologica Italiana 110, 581–600.

Lay, T., Wallace, T.C., 1995. Modern Global Seismology. Academic Press (521pp).

Lin, J., Stein, R., 2004. Stress triggering in thrust and subduction earthquakes, and stress interaction between the southern San Andreas and nearby thrust and strike-slip faults. J. Geophys. Res. 109, B02303. http://dx.doi.org/10.1029/2003JB002607.

Lin, J., Stein, R.S., Meghraoui, M., Toda, S., Ayadi, A., Dorbath, C., Belabbes, S., 2011. Stress transfer among en echelon and opposing thrusts and tear faults: triggering caused by the 2003 Mw = 6.9 Zemmouri, Algeria, earthquake. J. Geophys. Res. 116, B03305. http://dx.doi.org/10.1029/2010JB007654.

Maesano, F.E., D'Ambrogi, C., Burrato, P., Toscani, G., 2015. Slip-rates of blind thrusts in slow deforming areas: examples from the Po plain (Italy). Tectonophysics 643, 8–25. http://dx.doi.org/10.1016/j.tecto.2014.12.007.

Mantovani, E., Babbucci, D., Tamburelli, C., Viti, M., 2009. A review on the driving mechanism of the Tyrrhenian-Apennines system: implications for the present seismotectonic setting in the Central-Northern Apennines. Tectonophysics 476, 22–40.

Mantovani, E., Viti, M., Babbucci, D., Albarello, D., Cenni, N., Vannucchi, A., 2010. Long-term earthquake triggering in the Southern and Northern Apennines. J. Seismol. 14, 53–65. http://dx.doi.org/10.1007/s10950-008-9141-z.

Margottini, C., Ambraseys, N.N., Screpanti, A., 1993. La magnitudo dei terremoti italiani del XX Secolo. E.N.E.A. Internal Publication, Rome (57 pp).
Martini, I.P., Sagri, M., 1993. Tectono-sedimentary characteristics of late Miocene-Quaternary extensional basins of the Northern Apennines, Italy. Earth Sci. Rev. 34, 197–233.
Métivier, L., de Viron, O., Conrad, C.P., Renault, S., Diament, M., Patau, G., 2009. Evidence of earthquake triggering by the solid earth tides. Earth Planet. Sci. Lett. 278, 370–375.
Michetti, A.M., Serva, L., Vittori, E., 2000. ITHACA Italy hazard from capable faults: a database of active faults of the Italian onshore territory, CD-ROM and explication notes (Eds.).
Michetti, A.M., Giardina, F., Livio, F., Mueller, K., Serva, L., Sileo, G., Vittori, E., Devoti, R., Riguzzi, F., Carcano, C., Rogledi, S., Bonadeo, L., Brunamonte, F., Fioraso, G., 2012. Active compressional tectonics, Quaternary capable faults, and the seismic landscape of the Po Plain (northern Italy). Ann. Geophys. 55 (5), 969–1001. http://dx.doi.org/10.4401/ag-5462.
Molli, G., Torelli, L., Storti, F., 2016. The 2013 Lunigiana (Central Italy) earthquake: seismic source analysis from DInSar and seismological data, and geodynamic implications for the northern Apennines. A discussion. Tectonophysics 668–669, 108–112.
Nostro, C., Stein, R.S., Cocco, M., Belardinelli, M.E., Marzocchi, W., 1998. Two-way coupling between Vesuvius eruptions and southern Apennine earthquakes, Italy, by elastic stress transfer. J. Geophys. Res. 103, 24487–24504. http://dx.doi.org/10.1029/98JB00902.
Oddone, E., 1918. Il terremoto dell'alta Valle del Tevere del 26 aprile 1917. Bollettino della Società Sismologica Italiana 21, 9–27.
Okada, Y., 1992. Internal deformation due to shear and tensile faults in a half-space. Bull. Seismol. Soc. Am. 82, 1018–1040.
Pantosti, D., Valensise, G., 1990. Faulting mechanism and complexity of the November 23, 1980, Campania-Lucania earthquake, inferred from surface observations. J. Geophys. Res. 95, 15,319–15,341.
Philippon, M., Willingshofer, E., Sokoutis, D., Corti, G., Sani, F., Bonini, M., Cloetingh, S., 2015. Slip re-orientation in oblique rifts. Geology 43, 147–150. http://dx.doi.org/10.1130/G36208.1.
Piana Agostinetti, N., Lucente, F.P., Selvaggi, G., Di Bona, M., 2002. Crustal structure and Moho geometry beneath the Northern Apennines (Italy). Geophys. Res. Lett. 29 (20), 1999. http://dx.doi.org/10.1029/2002GL015109.
Piccardi, L., Corti, G., Boccaletti, M., 1999. Oblique extension in the Tyrrhenian side of the Northern Apennines (Italy. Proceedings of the XXIV European Geophysical Society General Assembly, the Hague, 19–23 April 1999, Geophysical Research Abstracts, 1. Vol. 82.
Piccardi, L., Sani, F., Bonini, M., Boccaletti, M., Moratti, G., Gualtierotti, A., 1997. Deformazioni quaternarie nell'Appennino Centro-Settentrionale: evidenze ed implicazioni. Il Quaternario 10 (2), 273–280.
Piccinini, D., Piana Agostinetti, N., Roselli, P., Ibs-von Seht, M., Braun, T., 2009. Analysis of small magnitude seismic sequences along the Northern Apennines (Italy). Tectonophysics 476, 136–144.
Piccinini, D., Piana Agostinetti, N., Saccorotti, G., Fiaschi, A., Matassoni, L., Morelli, M., 2014. Orogen-parallel variability in 3D seismicity distribution, Northern Apennines (Italy): evidence for a slab tear fault? J. Geodyn. 82, 110–117.
Picotti, V., Ponza, A., Pazzaglia, F.J., 2009. Topographic expression of active faults in the foothills of the Northern Apennines. Tectonophysics 474, 285–294.
Pieri, M., Groppi, G., 1981. Subsurface geological structure of the Po plain, Italy. Publication 414. Consiglio Nazionale delle Ricerche, AGIP, Rome.
Reasenberg, P.A., Simpson, R.W., 1992. Response of regional seismicity to the static stress change produced by the Loma Prieta earthquake. Science 27, 1687–1690.
Ripepe, M., Marchetti, E., Delle Donne, D., Coli, M., Genco, R., Ulivieri, G., Colò, L., Lacanna, G., 2008. La Rete Sismica Locale dell'alto Mugello (Marzo-Luglio 2008). Dipartimento di Scienze della Terra di Firenze, Centro di Competenza del Dipartimento della Protezione Civile della Presidenza del Consiglio dei Ministri (48 pp).
Roberts, G.P., Michetti, A.M., 2004. Spatial and temporal variations in growth rates along active normal fault systems: an example from Lazio-Abruzzo, central Italy. J. Struct. Geol. 26, 339–376.
Rossi, M., Rogledi, S., Barbacani, G., Casadei, D., Iaccarino, S., Papani, G., 2002. Tectono-stratigraphic architecture of Messinian piggyback basins of northern Apennines: the Emilia folds in the Reggio-Modena area and comparison with the Lombardia and Romagna sectors. Bollettino della Società Geologica Italiana Spec. Vol. 1, 437–447.
Rovida, A., Camassi, R., P., G., Stucchi, M., 2011. CPTI11, the 2011 Version of the Parametric Catalogue of Italian Earthquakes, Milano, Bologna. http://dx.doi.org/10.6092/INGV.IT-CPTI11http://emidius.mi.ingv.it/CPTI11/ (Eds.).
Sani, F., Bonini, M., Piccardi, L., Vannucci, G., Delle Donne, D., Benvenuti, M., Moratti, G., Corti, G., Montanari, D., Sedda, L., Tanini, C., 2009. Late Pliocene–Quaternary evolution of outermost hinterland basins of the Northern Apennines (Italy), and their relevance to active tectonics. Tectonophysics 476, 336–356.
Scognamiglio, L., Tinti, E., Michelini, A., 2009. Real-time determination of seismic moment tensor for the Italian region. Bull. Seism. Soc. Am. 99, 2223–2242 (up-to-date catalogue at) http://earthquake.rm.ingv.it/tdmt.php.
Scrocca, D., Carminati, E., Doglioni, C., Marcantoni, D., 2007. Slab retreat and active shortening along the central-northern Apennines. In: Lacombe, O., Lavé, J., Roure, F., Verges, J. (Eds.), Thrust Belts and Foreland Basins: from Fold Kinematics to Hydrocarbon Systems. Frontiers in Earth Sciences. Springer, Berlin, pp. 471–487.
Sibson, R.H., 2000. Fluid involvement in normal faulting. In: Cello, G., Tondi, E. (Eds.), The Resolution of Geological Analysis and Models for Earthquake Faulting Studies. Journal of Geodynamics Vol. 9, pp. 469–499.
Solarino, S., 2005. The role of instrumental versus macroseismic locations for earthquakes of the last century: a discussion based on the seismicity of the North-Western Apennines (Italy). Ann. Geophys. 48, 923–936.
Stein, R.S., 1999. The role of stress transfer in earthquake occurrence. Nature 402, 605–609.
Stein, R.S., King, G.C.P., Lin, J., 1992. Change in failure stress on the southern San Andreas fault system caused by the 1992 magnitude 5 7.4 Landers earthquake. Science 258, 1328–1332.
Stramondo, S., Vannoli, P., Cannelli, V., Polcari, M., Melini, D., Samsonov, S., Moro, M., Bignami, C., Saroli, M., 2014. X- and C-Band SAR surface displacement for the 2013 Lunigiana earthquake (Northern Italy): a breached relay ramp? IEEE Journal of Selected Topics in Applied Earth Observations and Remote Sensing 7, 2746–2753. http://dx.doi.org/10.1109/JSTARS.2014.2313640.
Tanaka, S., Ohtake, M., Sato, H., 2004. Tidal triggering of earthquakes in Japan related to the regional tectonic stress. Earth Planets Space 56, 511–515.
Tanini, C., 1998. Tettonica attiva dell'Appennino centro-settentrionale compreso fra le province di Arezzo, Perugia e Terni. Università degli Studi di Firenze (Unpublished PhD Thesis, 67 pp. (with maps).
Toda, S., Stein, R.S., Richards-Dinger, K., Bozkurt, S., 2005. Forecasting the evolution of seismicity in southern California: animations built on earthquake stress transfer. J. Geophys. Res. 110, B05S16. http://dx.doi.org/10.1029/2004JB003415.
Toda, S., Stein, R.S., Sevilgen, V., Lin, J., 2011. Coulomb 3.3 Graphic-Rich Deformation and Stress-Change Software for Earthquake, Tectonic, and Volcano Research and Teaching — User Guide. U.S. Department of the Interior, U.S. Geological Survey, Open-File Report 2011–1060 (63 pp).
Valensise, G., Pantosti, D. (Eds.), 2001. Database of potential sources for earthquakes larger than M 5.5 in ItalyAnn. Geophys. 44 (4) (with CD-ROM).
Vannoli, P., Basili, R., Valensise, G., 2004. New geomorphic evidence for anticlinal growth driven by blind-thrust faulting along the northern Marche coastal belt (central Italy). J. Seismol. 8, 297–312.
Vannoli, P., Burrato, P., Valensise, G., 2015a. The seismotectonics of the Po Plain (Northern Italy): Tectonic diversity in a blind faulting domain. Pure Appl. Geophys. 172, 1105–1142. http://dx.doi.org/10.1007/s00024-014-0873-0.
Vannoli, P., Vannucci, G., Bernardi, F., Palombo, B., Ferrari, G., 2015b. The source of the 30 October 1930 Mw 5.8 Senigallia (Central Italy) earthquake: a convergent solution from instrumental, macroseismic, and geological data. Bull. Seismol. Soc. Am. 105, 1548–1561. http://dx.doi.org/10.1785/0120140263.
Viti, M., Mantovani, E., Cenni, N., Vannucchi, A., 2012. Post-seismic relaxation: an example of earthquake triggering in the Apennine belt (1915–1920). J. Geodyn. 61, 57–67.
Wells, D.L., Coppersmith, K.J., 1994. New empirical relationships among magnitude, rupture length, rupture width, rupture area, and surface displacement. Bull. Seismol. Soc. Am. 84, 974–1002.